אוניברסיטת תל-אביב
הפקולטה למדעים מדוייקים
ע"ש ריימונד ובברלי סאקלר

השתנות קווי הפליטה בקוואזרי פלומר-גרין

חיבור זה הוגש כחלק מהדרישות לקבלת התואר
"מוסמך אוניברסיטה" - .M.Sc באוניברסיטת תל-אביב
בית הספר לפיסיקה ואסטרונומיה

על-ידי

שי כספי

העבודה הוכנה בהדרכתו של פרופסור חגי נצר

מרץ 1994

תקציר

עבודת מחקר זו מתארת תכנית ניטור ספקטרופוטומטרית של תת-מדגם של 28 אוביקטים מתוך המדגם של קוואזרי פלומר-גרין. מטרת התכנית היא לבדוק את ההתאמה בין השינויים בקרינת הרצף לשינויים בקרינת קווי הפליטה ולקבוע את סקלת הזמן הרלוונטית למיפוי אזורי הקווים הרחבים בגרעיני גלקסיות פעילים בעלי בהירות גבוהה.

במחצית הקוואזרים נמצאו שינויים בפליטת הרצף בעלי אמפליטודה בטווח של 20-75%. זמני העליה והירידה של השינויים בפליטת הרצף הם מסדר גודל של 0.5-2 שנים. ברוב האובייקטים בעלי השינוי בפליטת הרצף נמצאו גם שינויים מתאימים בקווי הפליטה הרחבים $H\alpha$ ו $H\beta$. אמפליטודת השינוי בקווים קטנה בדרך כלל פי 2-4 מאמפליטודת השינוי ברצף.

עקומות אור וניתוח ספקטרלי מוצגים עבור שישה מן הקוואזרים המשתנים בעלי בהירות של $0.3\text{-}4X10^{45}$ ארג לשניה בתחום של 1000-10000 אנגסטרם. בארבעה מתוך אוביקטים אלו קווי הפליטה הגיבו לשינוי בעוצמת הרצף עם פיגור בזמן שהוא באותו סדר גודל או קטן מזמן הדגימה האופיני (מספר חדשים). התוצאות התצפיתיות נותחו בעזרת טכניקת המתאם המוצלב (Cross-Correlation) ובעזרת סימולציות מונטה-קרלו. נמצא כי השינויים בקווי הפליטה מפגרים אחר השינויים בפליטת הרצף עם זמן-פיגור של כ- 70 ימים, דבר המעיד על גודל אופיני לאזור הקווים הרחבים של כ- 70 ימי-אור. בנוסף, תוצאות ראשוניות מראות כי גודל אזור הקווים הרחבים בגרעיני גלקסיות פעילים מכויל בהתאמה לבהירות האוביקט.

בשניים מהקוואזרים לא הובחנו שינויים בקווים למרות שינויים בעלי אמפליטודה גדולה יחסית בפליטת הרצף. יתכן שזה מקרה קיצוני של תופעת תת ההגבה של הקווים שהובחנה בקוואזרים האחרים.

שיטה חדשה שלא נוסתה לפני כן של "סימולציה של סדרת גאומטריות" מוצגת כאן. שיטה זו מאפשרת לבדוק את גאומטרית אזור הקווים הרחבים ע"י שינוי פרמטר בגאומטריה. נימצא כי עבור מודל שבו פקטור הכיסוי פרופורציונלי לרדיוס אזור הקווים הרחבים בחזקת -5/6, תוצאות התצפיות על קווזרי פלומר-גרין עיקביות עם אזור קווים רחבים בעל גאומטריה של קליפה כדורית בעובי של כמה מאות ימי-אור.

Zheng et al. 1987, Ap. J., **322**, 164.

Zheng, W., 1988, Ap. J., **324**, 801.

O'Brian, P.T. and Harris, T.J., 1991, M.N.R.A.S., **250**, 133, 250.

Osterbrock, D.E., and Shuder, J.M., 1982, Ap. J., **49**, 149.

Penston, B.M., 1991, in *Variability of Active Galaxies*, eds. Duschl, W.J., Wagner, S.J., and Camenzind, M. (Springer-Verlag), p. 47.

Pérez, E., Penston, M.V., and Moles, M., 1989, M.N.R.A.S., **239** 55, 75.

Peterson, B.M., Crenshaw, D.M., and Meyers, K.A., 1985, Ap. J., **298**, 283.

Peterson, B.M., 1988, P.A.S.P, **100**, 18.

Peterson, B.M., et al., 1991, Ap. J., **368**, 119.

Peterson, B.M., 1993, P.A.S.P, **105**, 207.

Peterson, B.M., and Cota, S.A., 1987, A. J., **94**, 7.

Peterson, B.M., and Cota, S.A., 1988, Ap. J., **330**, 111.

Salamanca, et. al., 1993, Astro. Ap.

Schmidt M., and Green, R.F., 1983, Ap. J., **269**, 352.

Shastri, P., Wilkes, B.J., Elvis, M., and McDowell, J., 1993, Ap. J., **410**, 29.

Stirpe, G.M., 1991, Astro. Ap., **247**, 3.

Stirpe, G.M., et. al., 1994, Astro. Ap., in press.

Stirpe, G.M., et. al., 1994b, Ap. J., **425** in press.

Ulrich, M.H., Courvoisier, T.J.-L., and Wamsteker, W., 1988, Astro. Ap., **204**, 21.

Ulrich, M.H., Boksenberg, A., Bromage, G.E., Clavel, J., Elvis, A., Penston, M.V., Perola, G.C., and Sunders, M.A.J., 1991, Ap. J., **382**, 483.

Ulrich, M.H., Courvoisier, T.J.-L., and Wamsteker, W. 1993, Ap. J., **411**, 125.

Usher, P.D., 1978, Ap. J., **222**, 40.

Woltjer, L., 1990, in *Active Galactic Nuclei*, by R.D. Blandford, H. Netzer and L. Woltjer, eds. Courvoisier, T.J.-L., and Mayor M. (Springer-Verlag), p. 1.

Wanders, I., et. al., 1993, Astro. Ap., **269**, 39.

Yates , M.G., and Garden, R.P., 1989, M.N.R.A.S., **241**, 167.

Zamorani, G., Giommi, P., Maccacaro, T., and Tananbaum, H., 1984, Ap. J., **278**, 28.

Zheng, W., and Burbidge E.M., 1986, Ap. J. Lett., **306**, L67.

Gaskell, C.M., and Peterson, B.M., 1987, Ap. J. Suppl. **65**, 1.

Gondhalekar, D.M., et al. 1986, M.N.R.A.S., **222**, 71.

Gondhalekar D.M., 1990, M.N.R.A.S., **243**, 443.

Grandi, S.A., and Tifft, W.G., 1974, P.A.S.P., **86**, 873.

Hooimeyer, J.R.A., Miley, G.K., de Waard, G.J., and Schilizzi, R.T., 1992, Astro. Ap., **261**, 9.

Jacson, N., et al., 1992, Astro. Ap., **262**, 17.

Keel, W.C., and Allan, P.M., 1991, in *Variability in AGNs*, eds. H.R. Miller and P.J. Wiita, (Cambridge), p. 83.

Korista, K.T., A.J., 1991, **102**, 41.

Lawrence, A., 1987, PASP, **99**, 30.

Maoz, D. and Netzer, H., 1989, M.N.R.A.S., **236**, 21.

Maoz, D., Netzer, H., Leibowitz, E. ,Brosh, N., Laor, A., Mendelson, H., Beck, S., Mazeh, Z., and Almoznino, E., 1990, Ap. J., **351**, 75.

Maoz, D., Netzer, H., Leibowitz, E. ,Brosh, N., Laor, A., Mendelson, H., Beck, S., Almoznino, E., and Mazeh, Z., 1991, Ap. J., **367**, 493. Maoz, D., et. al., 1993, Ap. J., **404**, 576.

Maoz, D., Smith, P.S., Jannuzi, B.T., Kaspi, S., and Netzer, H., 1994, Ap. J., **421**, 34.

Neugebauer, G., Green, R.F., Matthews, K., Schmidt, M., Soifer, B.T., and Bennett, J., 1987, Ap. J. S., **63**, 615.

Netzer. H., et al., 1990, Ap. J., **353**, 108.

Netzer, H., 1990, in *Active Galactic Nuclei*, by R.D. Blandford, H. Netzer and L. Woltjer, eds. Courvoisier, T.J.-L., and Mayor M. (Springer-Verlag), p. 57.

Netzer, H., 1991, in *Variability of Active Galaxies*, eds. Duschl, W.J., Wagner, S.J., and Camenzind, M. (Springer-Verlag), p. 107.

Netzer, H., 1992, in *Contributions to the Madrid Conference on the Nearest Active Galaxies*, p. 15.

O'Brian, P.T., Gondhalekar, P.M., and Wilson, R., 1988, M.N.R.A.S., **233**, 801, 845.

References

Alloin, D., Pelat, D., Phillips, M.M, and Whittle, M., 1985, Ap. J., **288**, 205.

Alloin, D., Pelat, D., Phillips, M.M, Fosbury, R.A.E. and Freeman, K., 1986, Ap. J., **308**, 23.

Alloin, D., Boisson, C., and Pelat, D., 1988 Astro. Ap., **200**, 17.

Antonucci, R.R.J., and Cohen, R.D., 1983, Ap. J., **271**, 564.

Bahcall, J.N., Kozlovsky, B., and Salpeter, E.E., 1972, Ap. J., **171**, 467.

Berriman, G., Schmidt, G.D., West, S.C., and Stockman, H.S. 1990, Ap. J. S., **74**, 869.

Blandford, R.D., 1990, in *Active Galactic Nuclei* , by R.D. Blandford, H. Netzer and L. Woltjer, eds. Courvoisier, T.J.-L., and Mayor M. (Springer-Verlag), p. 161.

Blandford, R.D., and Mckee, C.F., 1982, Ap. J., **255**, 419.

Boroson, T., and Green, R., 1992, Ap. J. S.,

Clavel, J., and Wamsteker, W., 1987, Ap. J. Lett., **320**, L9.

Clavel, J., Wamsteker, W., and Glass, I.S., 1989, Ap. J., **337**, 236.

Clavel, J., et al. 1990, M.N.R.A.S., **246**, 668.

Clavel, J., et al. 1991, Ap. J., **366**, 64.

Courvoisier, T.J.-L. et al., 1990, Astro. Ap., **234**, 73.

Curri, R.M., and Wisniewski, W.Z., 1985, Ap. J., **296**, 423.

Edelson, R.A., and Malkan, M.A., 1987, Ap. J., **323**, 516.

Edelson, R.A., and Korlik, J.H., 1988, Ap. J., **333**, 646.

Evans, I.N., et. al. 1993, Ap. J., **417**, 82.

Fairall, A.P., 1977, M.N.R.A.S., **180**, 391.

Gaskell, C.M., and Spark, L. S., 1986, Ap. J., **305**, 175.

galaxies and with the unified scheme for AGNs. Preliminary results show that the BLR size scales with luminosity.

The "geometric series simulation" described in this study are new and were not attempted before. It was found that for a model with a covering factor given by $dc \propto r^{-5/6}$, the observations of the PG quasars are consistent with a thick shell BLR with thickness of few hundred light-days. Also, features of the models were demonstrated and it was found that for certain models the observational data obtained so far are inadequate, and more data are required. The new method of simulation can be performed on other geometries (like thin-disks, toruses etc.) to test their agreement with the observations and to examine their properties.

The PG monitoring is an on-going project, and more data will be obtained, hopefully up to 30 points in the light-curves. As it shown in this study, good observational results combined with cross-correlation analysis and simulation, can give meaningful results about the BLR structure in AGNs.

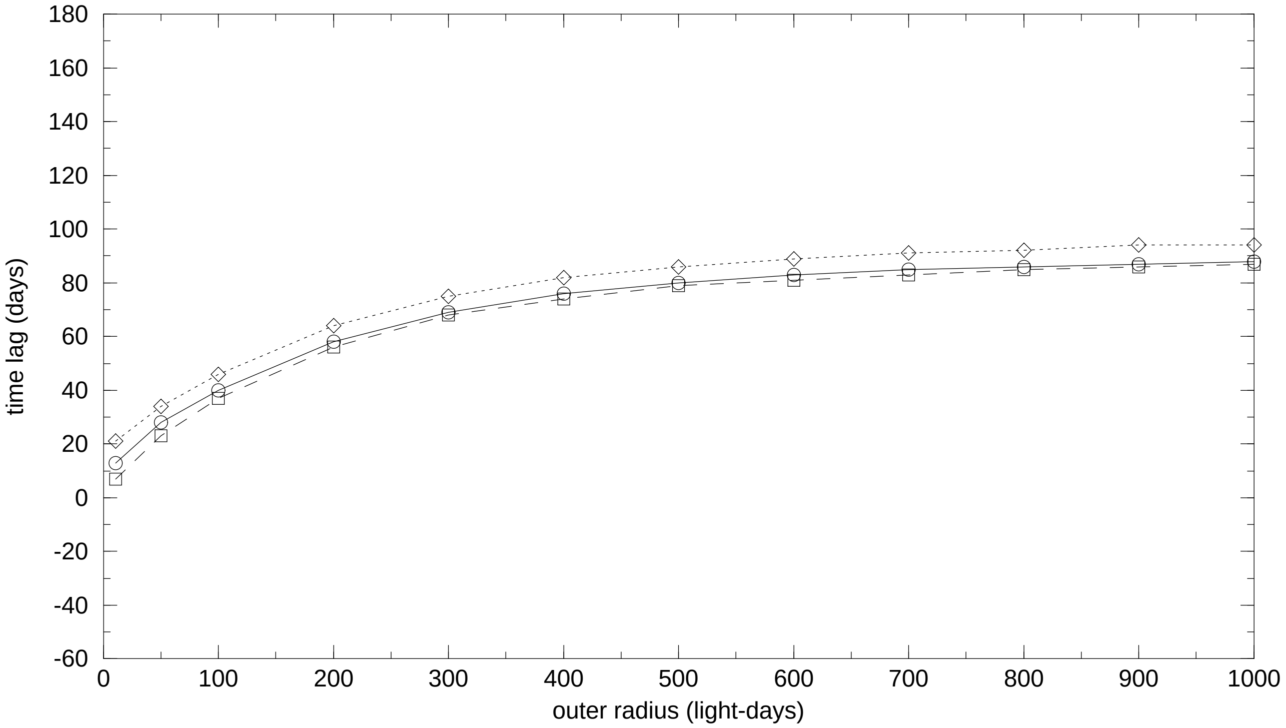

Figure 3.6: Same as Fig. 3.6 for light-curve sampling of 30 times. The 90% range is much narrower.

ures. 3.5 and 3.6 and are to be compared with Figures. 3.2 and 3.3. The width of the CCPD are much narrower and the peak is better defined so the error is much smaller. Also the rejection range in Figure 3.6 is much narrower, so a model can be rejected with higher confidence level.

3.3 Summary

Results of the monitoring project were analyzed using the cross-correlation method and Monte-Carlo simulations. Despite of the limited information and the resulting uncertainties in the CCFs, some conclusions can emerge. The main result is that variation in quasars continuum and the Balmer emission-lines were detected. For the first time it was established that the variation in the emission-lines are lagging behind the continuum variations. The time lag is of order 70 days, indicating a BLR with a typical size of 70 light-days. This is in agreement with BLR sizes deduced from observation of Seyfert 1

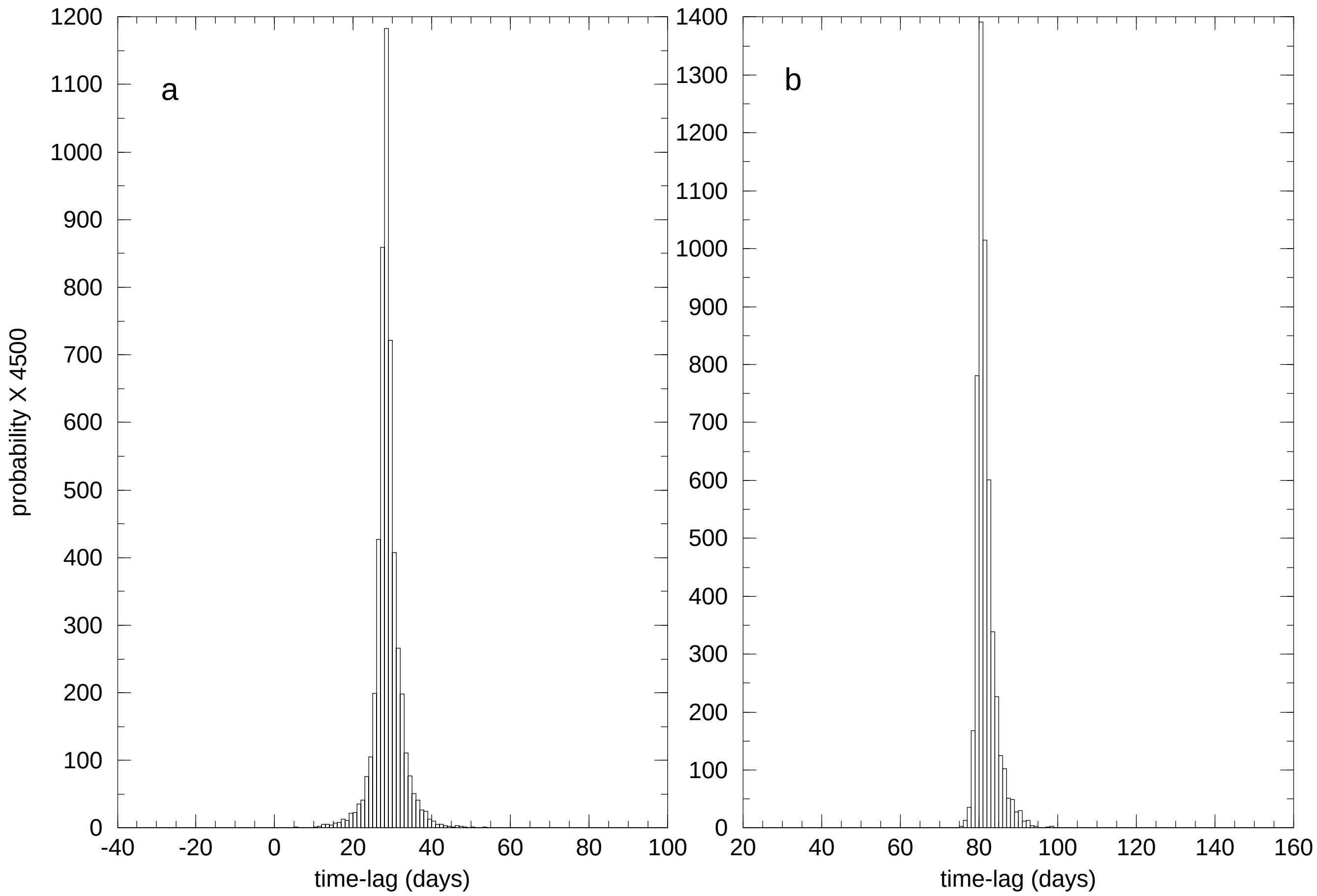

Figure 3.5: Same as Fig. 3.2 for line light-curve sampling of 30 times. The peaks are very well defined and the CCPDs are much narrower than in Figure 3.2.

with outer radius less than 20 light-days, and above 200 light-days can be ruled out with confidence level of 95%.

Simulation based on eqs. 3.8 and 3.9 that were carried out with inner radius of 50 light-days rejected all geometries with outer radius of above 150 light-days with confidence level of 95%. The simulation results when using inner radius of 5 light-days are the same as those illustrated in Figure 3.4 for inner radius of 10 light-days. This confirm the conclusion from eq. 3.9 that in this model outer radii contribute more to the line response than inner radii.

To illustrate the potential of the new simulations, it was run once more, this time sampling the line light-curve 30 times instead of 6. The results are illustrated in Fig-

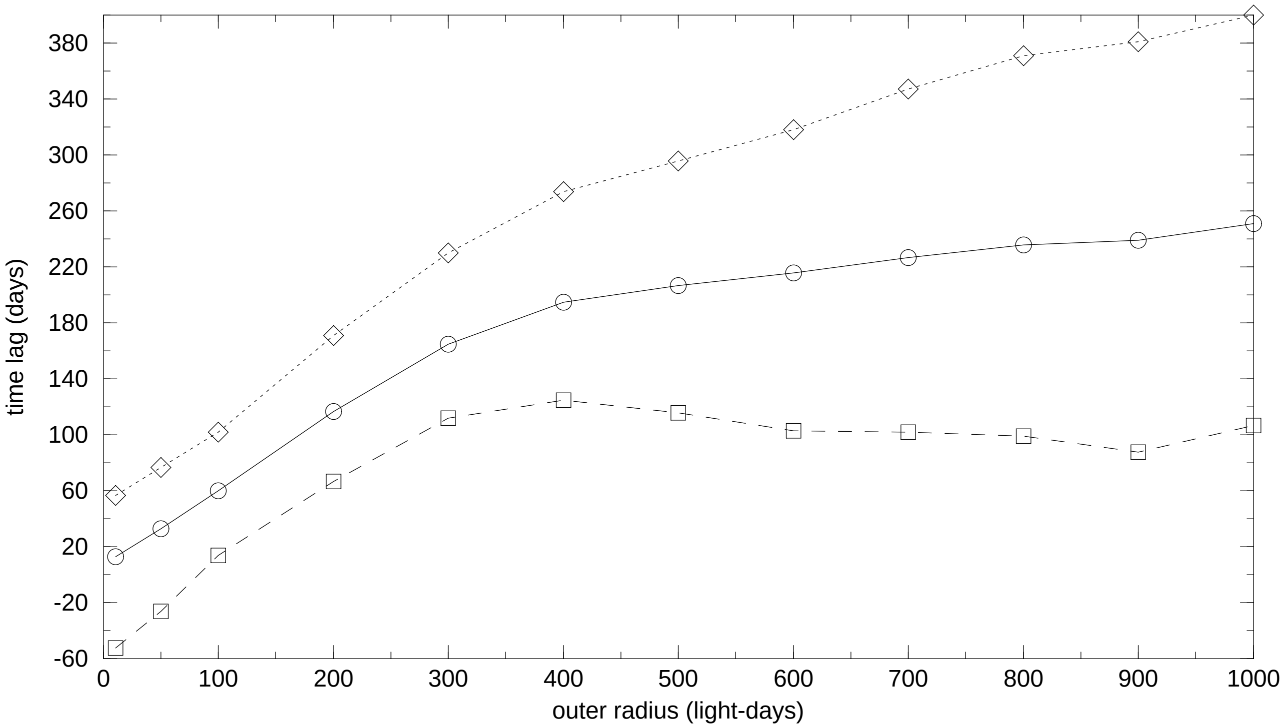

Figure 3.4: Same as Fig. 3.3 for a model with $dc \propto dr$. Note the change of slope and the larger 90% range for outer radii exceeding 300 light-days.

as a power of 1. This results in an increased time-lag as the outer radius increases (Figure 3.4).

As seen in Figure 3.4, in geometry of inner radius of 10 light-days and varying outer radius, the time-lags are increasing for all CCPDs up to outer radius of 300 light-days. For larger outer radii, the increase is slower. This may lead to the conclusion that outer radii beyond 300 light-days contribute less to the line response, in contrast to the expected from eq. 3.9. However the change of slope has a different cause. Note that the width of the CCPD for outer radii larger than 300 light-days is broad and becoming broader for larger outer radius (Figure 3.4). This is due to the fact that the time interval of the observation is only about 500 days, which is not enough for detecting lags that are larger than ~ 200 light-days. Thus, in this model, very little can be said about geometries with outer radii larger than 300 light-days. However, from the CCF time-lag found for $H\alpha$ and $H\beta$ emission-line of PG 0804+762 it can be concluded that in this model all geometries

beyond about 400 light-days contribute very little to the emission-line light-curve (Figure 3.3). This is expected from eq. 3.7, that shows that the contribution of a shell at radius r to the emission-line-flux is decreasing as a power of $-5/6$, and from the cumulative flux, E, in eq. 3.6 that depend on r_{out} increase only as a power of $1/6$. Hence, within this model a time-lag of about 100 light-days is expected for all BLRs with outer radius of above 400 light-days. The simulations show that the CCF time-lag found for the $H\alpha$ and $H\beta$ emission-lines of PG 0804+762 are in agreement with geometry of inner radius of 10 light-days and outer radius of 200 light-days (the CCPD is peaked at $\sim$ 60 light-days). However, those time-lags are also consistent with almost any other higher outer radius within the 90% range defined in Figure 3.3. All geometries of thick shell with inner radius of 10 light-days and outer radius up to 50 light-days can be ruled out for those emission-lines with a confidence level of 95%.

The same simulation (based on eq. 3.6), was run with inner radius of 5 light-days and varying outer radii. The results were similar to the ones described above for an inner radius of 10 light-days. Simulation with inner radius of 50 light-days and varying outer radii. show that all geometries with this inner radius and outer radii larger than 200 light-days can be ruled out with a 95% confidence level.

Different results can be obtained when running the model described in eqs. 3.2–3.6 with different parameters. This can be used to rule out certain models that do not fit the data with a high confidence level. This can be illustrated by assuming $s = 9/4$ in eq. 3.2, which will results in eq. 3.6 changing into:

$$N \propto r^{-9/4} , \qquad U \propto r^{1/4} , \qquad E \propto [(\frac{r_{out}}{r_{in}}) - 1]r_{in}, \qquad dC \propto dr , \tag{3.8}$$

i.e., the covering factor per unit shell thickness is constant all over the BLR. In this case Eq. 3.7 changes into,

$$\Psi(t) \propto \ln(r) , \tag{3.9}$$

which means that the outer shells of the thick shell will contribute to the emission-line intensity more than the inner shells. Also, The cumulative flux, E, depend on r_{out} increase

the number of times the line light-curve is sampled, and the shape of the continuum light curve. Hence, the error in the CCF time-lags of the emission-lines of PG 0804+762 can be evaluated from the simulations. The 90% range found for PG 0804+762 is of order $\sim$ 110 light-days (Figure 3.3). From that result an error of $\sim \pm 55$ light-days can be associate with the time-lags presented in Table 4 for PG 0804+762. Furthermore, as explained in Maoz and Netzer (1989) the equivalent of the 1σ uncertainty (i.e. the 68% probability range) can be estimated from the CCPD. This was done by finding the range around the CCPD peak which included 68% of the CCF peaks. For PG 0804+762 this range corresponds to $\sim \pm 45$ light-days. With some caution this error can also be assigned for the measured lags in other objects in, since the characteristic variations are quite similar in all quasars studied.

For the geometry of inner radius of 10 light-days it was found that, the BLR gas

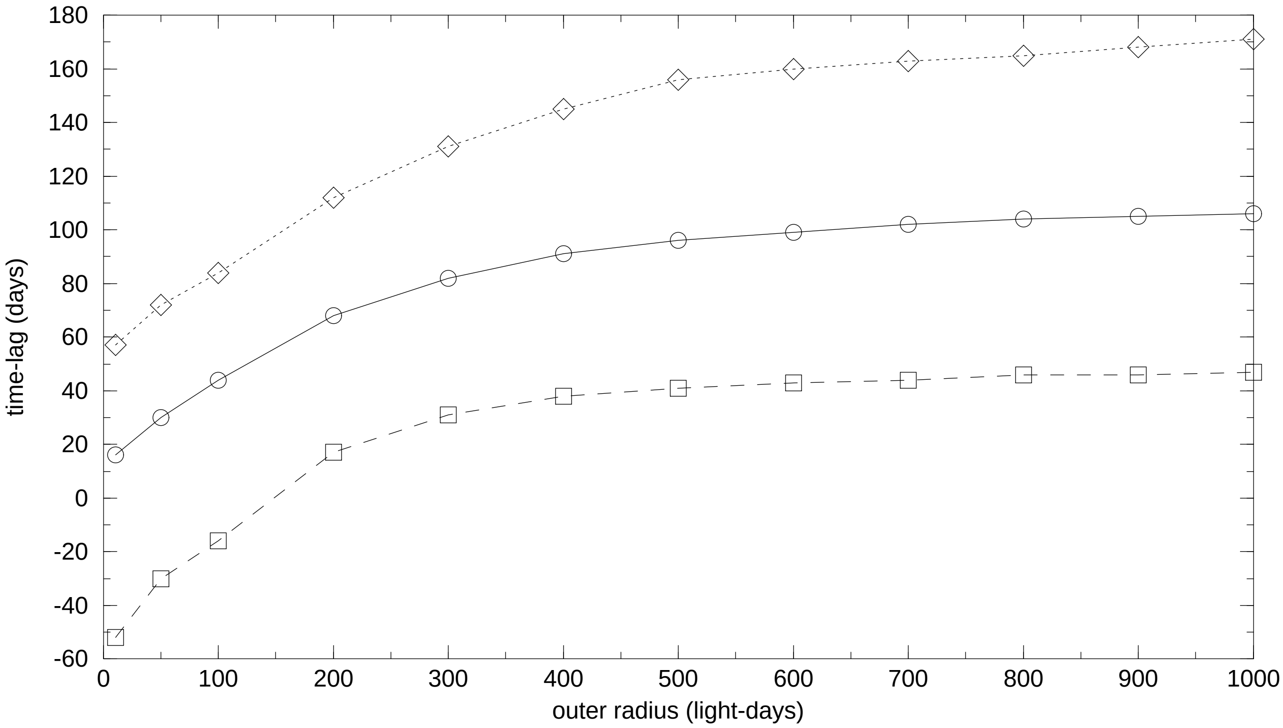

Figure 3.3: "geometric series simulation" for thick shell BLR with inner radius of 10 light-days and varying outer radius for the model with $dc \propto r^{-5/6}dr$. The line light-curve was sampled 6 times. Solid line is the CCPD peak, dashed line is the 5% time-lag, dotted line is the 95% time-lag. The range between the dotted and dashed lines is the 90% confidence range.

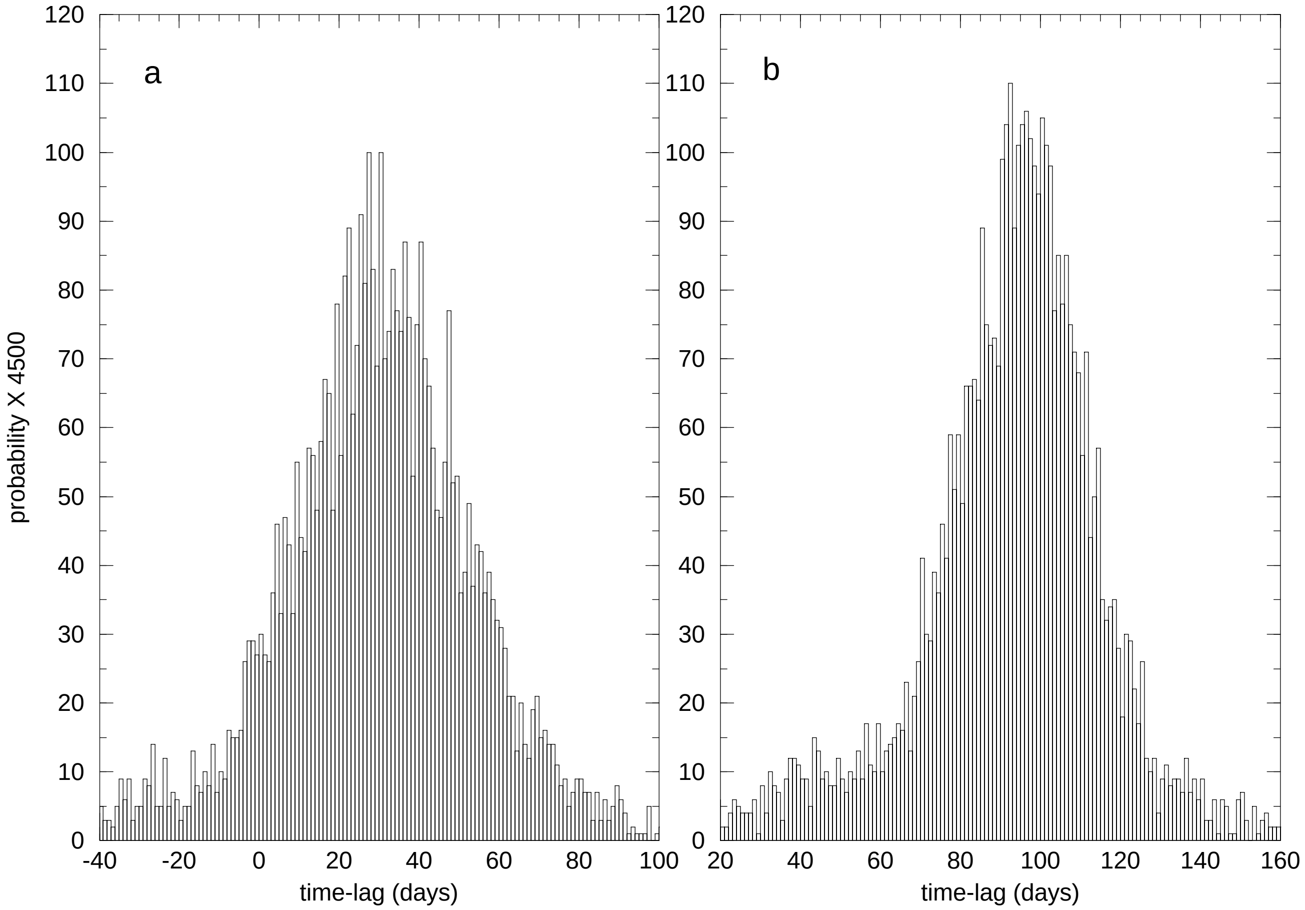

Figure 3.2: CCPD for thick shell BLR with inner radius of 10 light-days. The outer radius is 50 light-days (Figure a) and 500 light-days (Figure b). The line light-curve was sampled 6 times. The two CCPDs are very similar except for a shift by about 60 days.

six times, adding more iteration to the simulations will hardly improve it. Nevertheless, as can be seen, the peak of the CCPD is well defined.

For each CCPD, the 5% and the 95% time-lags were found from the simulations .The range between those two time-lags is the one that has 90% of the CCF peaks (this is illustrated in Figure 3.3). Hence if the model describes well the BLR properties, the CCF peak found from the observations will have 90% probability of falling in this range. This means that if the observed time-lags are out of this range we can role out this model (for the particular object) with 90% confidence level.

All CCPDs have about the same shape because the CCPD is mainly determined by

A reasonable choice (which is supported by observation) is $s = 1$, which gives

$$N \propto r^{-1} , \qquad U \propto r^{-1} , \qquad E \propto [(\frac{r_{out}}{r_{in}})^{1/6} - 1]{r_{in}}^{1/6}, \qquad dC \propto r^{-5/6} dr . \quad (3.6)$$

The transfer function produced from such a model has the following dependence on the BLR radius:

$$\Psi(t) \propto \int \frac{dC(r)}{r} \propto r^{-5/6} . \qquad (3.7)$$

This last relation was used in the simulation to produce the BLR response to the continuum variations.

For chosen inner and outer radius of the thick shell, the line light-curve was calculated using this model. This line light-curve was sampled randomly six times, which is the characteristic sampling of the observed line light-curves, and it is the number of times that PG 0804+762 was observed. The sampled points were linearly interpolated and cross-correlated with the continuum light-curve. The top 20% of the peak of the CCF was fitted with a second degree polynomial, the peak of which was taken as the time-lag of the cross-correlation. The process of sampling the light-curve and finding the time-lag from the cross-correlation was repeated about 4500 times to obtain a Cross-Correlation Peak Distribution (CCPD), which is the expected distribution of the time-lags. The peak of the CCPD was fitted with a second order polynomial and the maximum of the fit was taken as the most probable time-lag for the assumed BLR geometry. From the CCPD one can find the probability to observe a certain time-lag for a certain geometry, and to give rejection probabilities to other time-lags.

The above simulation was repeated for a given inner radius (measured in light-days) and a range outer radii from inner radius plus 1 light-day to 1000 light-days. This is the first time that such a "geometric series simulation" is presented, It enable us to examine the model properties and its agreement with the observations. Examples for the CCPD that were obtained for an inner radius of 10 light-days are presented in Figure 3.2. The CCPD for outer radius of 50 light-days (figure 3.2a), has a peak at 30 days. The CCPD for outer radius of 500 light-days (Figure 3.1b) has a peak at 96 days. The main reason that the CCPD are somewhat noisy is the fact that the line light-curve was sampled only

variation, to estimate the probability of detecting such variations, and to find the geometry that best fit the BLR geometry. The simulations by Gaskell and Peterson (1987) and Peterson and Cota (1988) were restricted to one particular geometry and assumed normal distribution of the cross-correlation peaks. Maoz and Netzer (1989) extended and generalized the simulation to more geometries and abandoned the assumption of normal distribution of the cross-correlation peaks. The simulation described below followed the technique of Maoz and Netzer (1989), and goes one step further in simulating a series of geometries by changing one parameter in the geometry.

To carry out the simulations, the continuum light-curve of PG 0804+762 was assumed to represent real typical continuum light-curve. It was linearly interpolated and then sampled every day. A spherical shell geometry with an optically thick gas was assumed for the BLR. The BLR model chosen is the one described in Netzer (1990) and in Netzer (1992), with the following properties:
The particle density is assumed to have a simple dependence on the BLR radius,

$$N \propto r^{-s} , \tag{3.2}$$

hence the ionization parameter, which specifies the ratio of the ionization photon flux to the gas density, obeys the relation,

$$U \propto r^{s-2} . \tag{3.3}$$

Assuming the BLR is compose of numerous small clouds with virial motion and overall mass conservation, the relation for the covering factor, which is the fraction of sky covered by photoionized gas clouds, as seen from the center, is

$$dC \propto r^{2/3s-3/2} dr . \tag{3.4}$$

Assuming line emission dependence in radius as r^{-2} (which is a good approximation for many lines), the cumulative line flux from the spherical shell, E, is

$$E \propto \int_{r_{in}}^{r_{out}} r^{-2} r^2 dC(r) \propto [(\frac{r_{out}}{r_{in}})^{2/3s-1/2} - 1] {r_{in}}^{2/3s-1/2} . \tag{3.5}$$

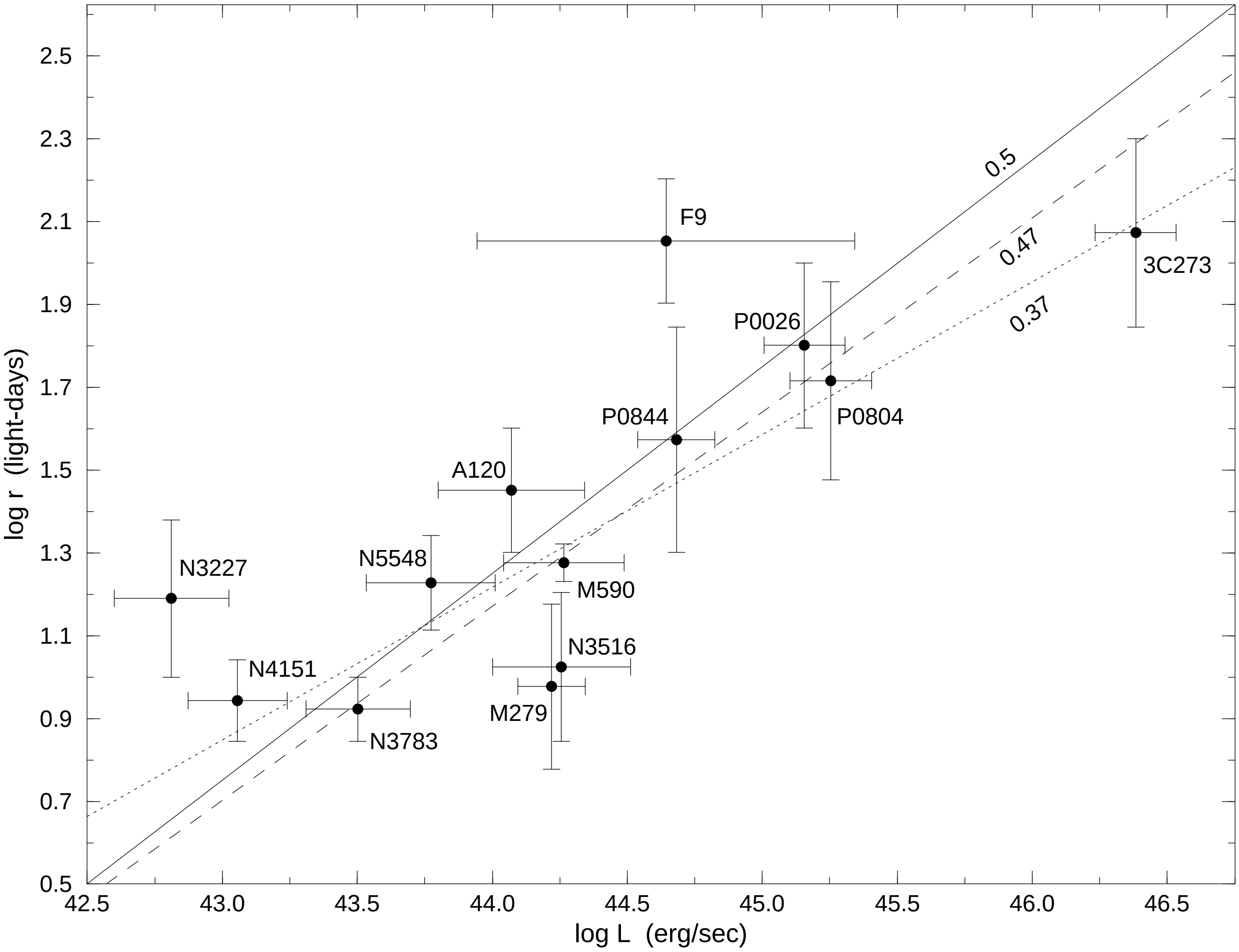

Figure 3.1: BLR radius-luminosity relationship for several AGNs. Luminosity between 0.1 − 1 μm, based (for most objects) on $F_\lambda(\sim 5000\mathring{A})$, and assuming $H_0 = 75$ km s^{-1}Mpc^{-1}, $q_0 = 0.5$, and a power-law continuum spectral index $\alpha_\nu = 0.5$. References: NGC 5548 Peterson 1993 and Maoz et. al. 1993, NGC 4151 Maoz et. al. 1991 and Clavel et. al. 1990, Mrk 279 Stirpe et. al. 1994 and Maoz et. al. 1990, Akn 120 Peterson 1988 and Peterson & Gaskell 1991, Mrk 590 Peterson et. al. 1993, NGC 3783 Stirpe et. al. 1994b, Fairall 9 Clavel et. al. 1989, 3C 273 O'Brian & Harris 1991, NGC 3227 Salamanca et. al. 1993, NGC 3516 Wanders et. al. 1993, PGs objects from this study.

3.2 Simulations

Monte-Carlo simulations are often used in order to examine the significance of the cross-correlation technique. The method assumes a certain geometry for the BLR and uses the simulation to predict the emission-line variation in response to a certain continuum

days.

The time-lags for all Balmer-lines are of order 50 – 150 days. This supports the claim from chapter 2 that the BLR size in quasars is of order of light months, and not of light years. Those time-lags are an order of magnitude larger than those found in Seyfert 1s, and indicate more extended BLRs in quasars, in accordance with the unified theory.

PG 0844+349, with the shortest time-lag, is the least luminous of the three quasars and the one showing the highest relative change in the continuum (highest $F_{max}/F_{min} - 1$ in Table 1). The luminosity and time-lag for PG 0844+349 are smaller than those of the other two quasars, and are bigger than the typical values of Seyfert 1 galaxies. This is an evidence that luminosity and BLR size are continuos along the AGN sequence. It is also consistent with the theoretical relation between the luminosity of the central source L, and the BLR size r,

$$r \propto L^{1/2} \tag{3.1}$$

(Peterson 1993). This relation is illustrated in Figure 3.1 for all published measurements which are "reasonably" well determined. As seen from the diagram, without our data all points but one are for Seyfert 1 galaxies and can be interpreted in various ways. The data presented in this study fill the gap between Seyferts and luminous quasars. A χ^2 fit was applied to the points. When the r errors were taken into account a 0.37 slope was found (dotted line), and when the L error were taken into account a 0.47 slope was found (dashed line). Both slops are consistent with 0.5 (solid line).

An interesting feature that arise from Table 4, is that in all three quasars, the $H\alpha$ variations are lagging behind the $H\beta$ variations. This is in contradiction to the results found for NGC 5548 (Peterson 1993), where the $H\beta$ lags behind the $H\alpha$ by 3 days, and also in disagreement with the results for NGC 4151 (Maoz et. al. 1991), where no lag between the lines was found. This feature can be caused by wrong or misleading interpolation and further monitoring is required to clarify this point.

Table 4: CCF time-lags

PG object	$H\alpha$ lag (days)	$H\beta$ lag (days)	$H\alpha$ lag behind $H\beta$ (days)	CCF maximum ± 0.05
(1)	(2)	(3)	(4)	(5)
0026+129	73 (80)	69 (68)	14 (31)	0.75 (0.95)
0804+762	141 (55)	67 (55)	71 (0)	0.93 (0.98)
0844+349	50 (13)	40 (11)	5 (3)	0.90 (0.95)

For each object in column 1, the $H\alpha$ time-lag (column 2) and the $H\beta$ time-lag (column 3) are given. The $H\alpha$ and $H\beta$ light-curves were also cross-correlated with each other and those results are given in column 4. The CCF peak-value is given in column 5 (this value is constant, within the error bars given, to all the CCFs of each quasar in the table). The numbers given without brackets are the ones that resulted from the above described linear interpolation. The numbers in brackets resulted from a different interpolation method between the light-curve points, which is described in the next paragraph.

In order to test the dependence of the CCF on the interpolation method, a polynomial interpolation method was also applied. Polynomial interpolation can introduce spurious features (i.e., local maxima and minima which have nothing to do with the observed points). Indeed, this was the case for PG 0026+129 and PG 0844+349 line light-curves, so the results for those objects should be treated with extra caution. The polynomial interpolation for the continuum light-curves and for the line light-curves of PG 0804+762, were in good agreement with the observed data. The results of the CCF from the polynomial interpolation are shown in Table 4 (in brackets). The $H\alpha$ lag of PG 0804+762 in the linear interpolation method is the largest, and is more than twice largeer than the $H\beta$ lag for this object. This outstanding results is disappearing when the polynomial interpolation method is applied, and both line CCFs of this object give the same lag, which is consistent with the lag found for $H\beta$ with the linear interpolation method. Thus, the $H\alpha$ lag is probably caused by wrong interpolation.

The widths of the CCFs, measured at the zero intensity (i.e. where the cross-correlation coefficient is 0) are of order of 300 days. The widths are mainly determined by the continuum ACF (see eq. 1.11) since the variability time-scale is of order of several hundred

Chapter 3

Cross-Correlations and Simulations

3.1 Cross-Correlation

The light-curves described in chapter 2 include only very few points, but the cross-correlation method can be applied to them. In order to perform the cross-correlation, the continuum light-curve and each of the line light-curves, of each quasar, were interpolated linearly. No extrapolation was done in order to avoid introducing artificial data. The interpolated light-curves were sampled with a regular time interval of 1 day and each of the line light curve ($H\alpha$ and $H\beta$) were cross-correlated with the continuum light curve using eq. 1.12. The top 20% of the peak of the CCF was fitted with a second degree polynomial, in order to minimize the effects of the interpolation method. The position of the peak of the polynomial was taken as the time-lag of the cross-correlation.

As noted in section 2.4, despite the detection of changes in the continuum flux, line-responses were not detected for PG 0953+414 and PG 1613+658. Thus the CCF for those objects did not show a peak, and a time-lag could not be determined. Also, the change in the continuum flux of PG 1229+204 was a gradual rise of 60%, and the Balmer line response was a gradual rise of $\sim$ 25% (section 2.3.5). Since both the continuum and the line light-curves show gradual rise, it was impossible to determine a time-lag for this quasar. The time-lags that were measured for the other three objects are listed in Table 4.

such lags.

From a practical viewpoint, the slow continuum variations that we have found to be typical to our sample mean that monitoring over several years is required in order to see several rise-and-fall "events" that will allow a secure measurement of the lag of the emission lines, and hence the size of the BLR. The apparently quick response of the lines means that good temporal sampling is also required. A further practical problem which has emerged from our study is the low variation amplitude of the lines, which makes highly accurate measurements important. Despite these difficulties, we have shown that quasar emission-line monitoring on small and medium-sized telescopes is feasible. Our monitoring program has already produced several interesting results on quasar emission-line variability. Our continued observations will hopefully further clarify the properties and structure of these AGNs.

Acknowledgements We are grateful to the staffs at Steward and at Wise Observatories for their expert assistance in this project. We thank E. Almoznino, Y. Goldberg, A. Heller, and H.-W. Rix for their help with the observations. A. Laor, B.M. Peterson, and the anonymous referee are thanked for helpful comments. We acknowledge support by NASA contract NAS 5-29293 and NASA grant NAG 5-1630 (P.S.S.), and by the US-Israel Binational Science Foundation through grant 89-00179 (H.N.). This research has made use of the NASA/IPAC Extragalactic Database (NED), which is operated by JPL, Caltech, under contract with NASA.

and Balmer-line variation amplitudes, and these two properties may be related. The α_{ox} of Seyfert 1 galaxies in general, and of NGC 5548 in particular, is smaller than the typical value for radio-quiet quasars, i.e., Seyfert galaxies are relatively stronger X-ray emitters (e.g. Shastri et al. 1993). The larger amplitude observed for the Balmer lines may reflect the conditions in the hard X-ray heated zone of the broad line gas. Non-linear response may also be observed if some of the continuum emission is beamed toward us, in a way that the BLR gas does not see the same continuum variations that we do. The class of optically-selected objects we are studying, however, is not generally associated with significant beaming.

Alternatively, a large BLR could cause low-amplitude line variations. In a large BLR, where the light-travel-time across the region t_{BLR} is much longer than the continuum variation timescale t_{con}, the line response is spread over a time $\sim t_{BLR}$ and is therefore reduced relative to the continuum variation amplitude by $\sim t_{con}/t_{BLR}$. In such a scenario, adequately-sampled data would also show a lag $\sim t_{BLR}$ of the lines behind the continuum. With additional data, it should be possible to distinguish non-linearity from large BLRs.

If, as is likely in NGC 5548, non-linearity is the explanation for the low amplitude of the line variations, the small lags of the emission-line light-curves of the four quasars with variable lines indicate that the BLR in quasars having such luminosities is smaller than ~ 1 lt-yr. This result is clearest in PG 0804+762 (Fig. 2.3), where the sampling and the characteristics of the light curves leave little doubt that the lines are following the continuum closely. Our work therefore confirms previous reports (see § 2.1) that the BLRs of quasars are smaller than originally predicted by photoionization models.

The 1000-10,000Å luminosity of the six objects under study is $0.3 - 4.4 \times 10^{45}$ erg s^{-1} (see Table 1). For comparison, the equivalent number for the Seyfert galaxy NGC 5548 is $\sim 6 \times 10^{43}$ erg s^{-1}, and for the luminous quasar 3C 273 it is about 2.6×10^{46} erg s^{-1}. The six quasars therefore have luminosities 5-70 times that of NGC 5548. If the BLR size scales roughly as $L^{1/2}$ (e.g. Netzer 1990), we expect, by scaling to the Peterson et al. (1991) results, line-to-continuum lags of 40-170 days. Our results are consistent with

studies. Our one exception to the low line variation phenomenon is PG 0804+762, in which the optical continuum and the Balmer lines vary with comparable amplitudes.

The relatively low amplitude of Balmer line response to ionizing continuum changes has already been observed in the Seyfert galaxy that has been most intensively monitored — NGC 5548 (Peterson et al. 1991). The optical nonstellar continuum and the Balmer lines in NGC 5548 vary with similar amplitudes, which are 2-3 times lower than the amplitude of the 1350Å continuum variations. The Balmer line variation amplitudes we observe in the quasars are 3-4 times lower than those of the *optical* continuum. An increase in continuum variation amplitude with shorter wavelength seems to be generic to Seyfert 1s and quasars (e.g. Kinney et al. 1991) and can be seen to a greater or lesser degree in the spectra of the quasars in Figs. 2.2-2.7. This implies that the phenomenon of low ratios of Balmer-line/ *ultraviolet*-continuum variation is much more pronounced in most of the quasars we have studied thus far than in NGC 5548. As already noted above, the extreme case is PG 1613+658, where by extrapolation, Figure 2.7a suggests the ionizing UV continuum varied by a factor of perhaps 3-5, with no detectable changes in Balmer line flux.

The low amplitude line variability we see in the quasars is a manifestation of either a degree of non-linearity in the response of the broad emission lines to continuum variations, or of a large BLR causing a "smearing-out" of the line variations.

Non-linear response of the broad-line gas can be caused by changes in the line production efficiency as a function of the changing ionization parameter. For example, a larger ionization parameter may increase the relative emission of $Ly\alpha$ and the strong ultraviolet resonance lines, at the expense of the Balmer lines. A similar effect can be caused by a change in the shape of the ionizing continuum when it varies. An indirect way to examine this possibility is to compare the ultraviolet and X-ray flux of the objects under study. Boroson and Green (1992) list α_{ox} for five of the six objects we study. PG 0804+762 has the smallest α_{ox} (1.34) while the other four have values between 1.43 and 1.53. PG 0804+762 is also the one object that shows comparable optical-continuum

2.4 Discussion

The present study is the first systematic attempt to investigate the line and continuum correlation in a complete sample of optically-selected quasars. The data presented in the previous section begin to address several of the problems at which our program is aimed. The continuum variability amplitudes listed in Table 1 confirm the results of Keel and Allan (1991) for the PG quasars as a whole. Our results show that the PG quasars in our sub-sample are a moderately-variable class of objects, that typically vary with amplitudes of 0% to 50% on a two-year timescale. Contrary to some popular views, the radio-loud quasars in the sample (PG 1100+772, PG 1202+281, PG 1226+023 [=3C 273], and PG 1512+270) are not noticeably more variable than the radio-quiet quasars. The continuum light curves shown for six of the quasars in Figs. 2.2-2.7 show that the the optical continuum usually undergoes slow and gradual changes, with typical rise or fall times of 0.5-2 years. Continued monitoring is required to confirm the generality of this result, and to accumulate a long enough temporal baseline for a more quantitative analysis.

The emission-line variability of the quasars shows some mixed behavior. Four out of the six quasars we have examined in detail show the Balmer lines to be varying in phase with the continuum (to within the temporal sampling resolution). In three out of the four quasars with variable lines, the amplitude of the line variations are 3-4 times smaller than those of the continuum. Continued observations will test whether the low line-variation amplitude is real, or the result of the undersampling of the emission-line light curves. Two of the six quasars show little or no line variations in response to the continuum changes. However, it is possible that the same effect of low-amplitude line variations is taking place in these two objects but with a slightly larger ratio of continuum to line variability amplitudes, such that the line variations fall below our detection threshold. For one of these two quasars with constant emission-line flux (PG 0953+414), we have presented measurements spanning a longer temporal baseline, showing that the near-constant line-flux behavior persists over a 5-year timescale. For the other (PG 1613+658), we have presented some evidence for constant line flux based on previous measurements by other

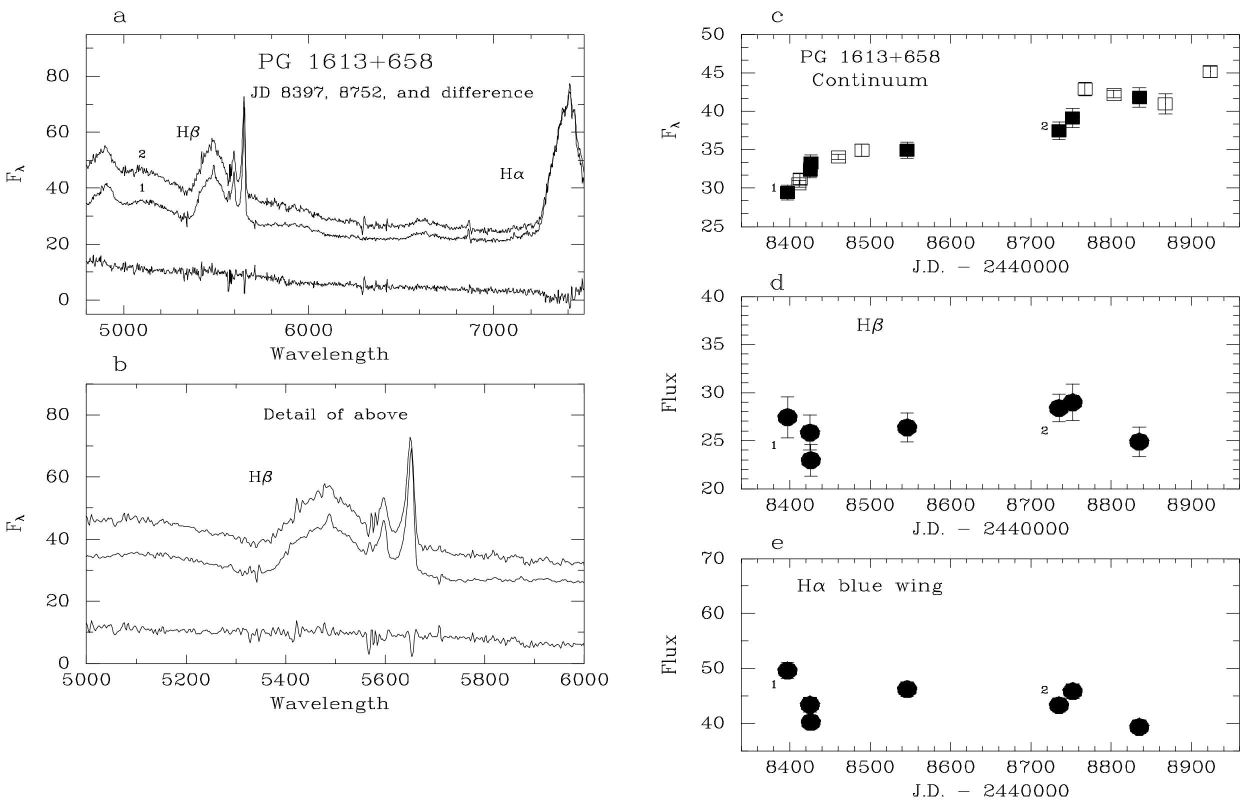

Figure 2.7: Same as Fig. 2.2 for PG 1613+653.

(As opposed to Seyfert galaxies, the host galaxy in quasars contributes negligibly to the total optical light, and so does not play a part in the hardening of the continuum as it brightens.)

Osterbrock and Shuder (1982) have previously reported for this quasar a continuum increase of 42% between two epochs separated by 3 years, with no $H\alpha$ variation and a $\sim 18\%$ change in $H\beta$. Their $H\beta$ measurement involved deblending of $H\beta$, [OIII], and FeII lines, and so could conceivably be consistent with no change in $H\beta$ strength. (They do not quote uncertainties or absolute fluxes.) Stirpe (1991) measured a 5000Å continuum flux in 1985 that was somewhat lower than the lowest one we find—2.5×10^{-15} erg s^{-1} cm^{-2} Å^{-1}, but an $H\beta$ flux of 2.57×10^{-13} erg s^{-1} cm^{-2}, in excellent agreement with the one we measure. It is therefore possible that the Balmer line flux remains unchanged in this quasar over long periods.

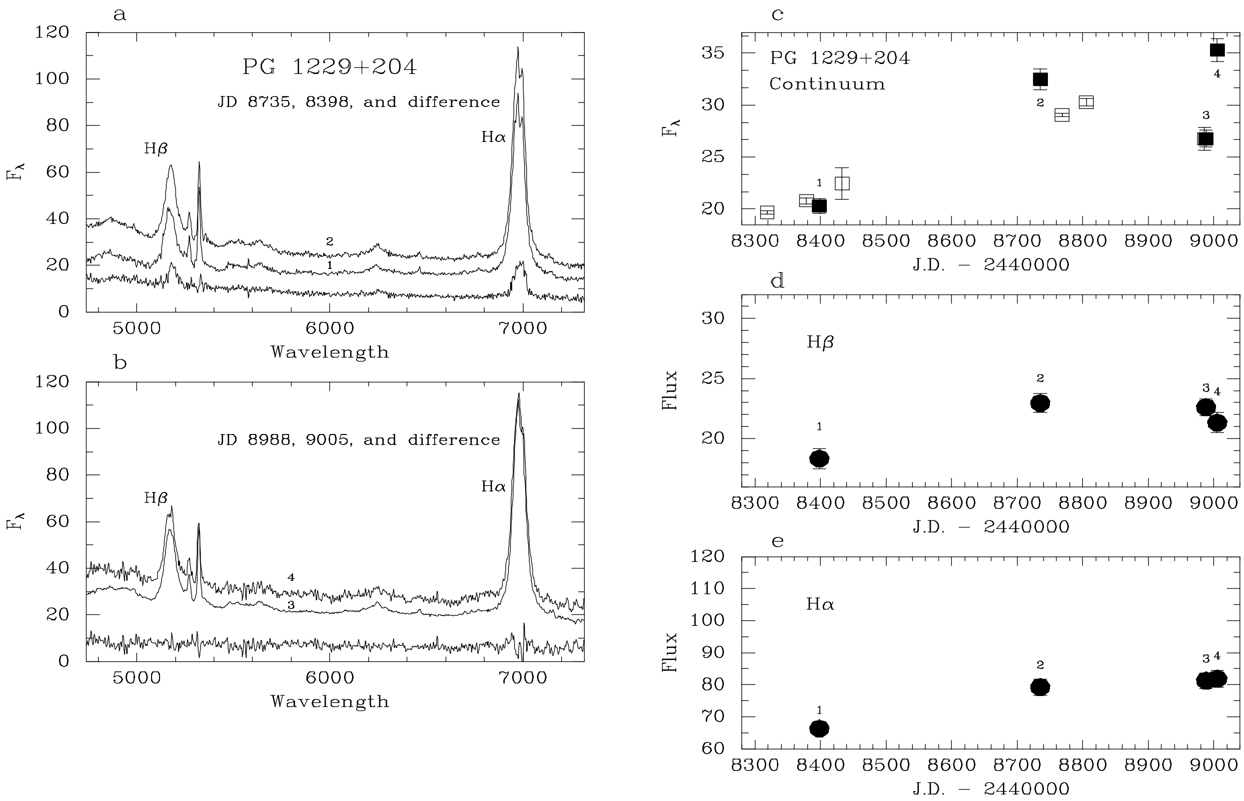

Figure 2.6: Same as Fig. 2.2 for PG 1229+204.

which, in the 17-day interval between the observations, is not reflected in the emission lines. Figure 2.6b shows the spectra from these epochs and their difference. Continued observations will show whether the non-response of the lines is the result of the non-zero lag behind the continuum, or whether such fast flares in the observed continuum are not seen in the ionizing continuum controlling the line-emitting gas.

2.3.6 PG 1613+658

The 5330Å continuum in this quasar (Fig. 2.7c) shows a slow rise by 50% over 525 days. As in PG 0953+414, no such trend is seen in the emission lines (Figs. 2.7d-e), which are constant to better than $\sim 10\%$. This is also seen in the spectra of the object, shown in Figure 2.7a. Note the degree to which the continuum becomes bluer as it brightens. This suggests that the UV ionizing continuum varies by an even larger amplitude than the optical continuum, and makes the non-response of the lines all the more puzzling.

of uncertainty in the continuum setting) allow only a looser upper limit of $\sim 30\%$ on the line variation.

We are also able to examine the longer-term behavior of this quasar from spectra taken during 1987-89 at the Wise Observatory, using the observational setup described by Maoz et al. (1989). The spectrophotometry was done relative to the same comparison star used in the present study. We have measured the continuum and line fluxes in the old spectra in the same way as in the spectra from the present work. Figs. 2.5d and 2.5e, combine the old measurements with the present measurements from Figs. 2.5b and 2.5c. The old measurements are noisy due to the lower efficiency of the setup, the shorter integration times, and the wider (20″) slit used in the past. Nevertheless, some interesting facts are revealed by the combined data with their five-year baseline. Fig. 2.5d shows that the mean continuum level in 1987-89 (J.D. 7145-7645) was slightly higher than the highest level reached in 1993 January (J.D.$\sim$ 9000). From Fig. 2.5e, we see that the mean $H\beta$ level in 1987-89 was $\sim 1.7 \times 10^{-13}$ erg s^{-1} cm^{-2}, very similar to the $H\beta$ flux in 1993 January. The line variation in this object is therefore much smaller than the continuum variation, even when they are followed for 5 years.

2.3.5 PG 1229+204

This is the lowest luminosity object in our sample, with about 6 times the average luminosity of NGC 5548. Previous work indicated little or no variability in this object (Osterbrock and Shuder 1982; Peterson, Crenshaw, and Meyers 1985; Yates and Garden 1989). In contrast, the quasar underwent the largest continuum variations in our sample, with a variation amplitude of 75%. The spectra plotted in Figure 2.6a, and the first two spectral measurements in the light curves (filled squares and circles in Figs. 2.6c-e) show a clear Hα and Hβ response to the initial continuum rise. As in most of the variable objects, the line response to the 60% initial rise in the 5070Å continuum is only 25% in Hβ and 20% in Hα.

The last two epochs in our light curves show an increase by 30% of the continuum,

2.3.4 PG 0953+414

This is the most luminous quasar discussed here, with L(0.1-1μm)$\sim 4.4 \times 10^{45}$ erg s^{-1}, about 70 times the luminosity of NGC 5548. It is also one of two quasars (the second is PG 1613+658) where we measure large continuum variations accompanied by little or no Balmer-line response. Figure 2.5a shows spectra of PG 0953+414 at three epochs, and the difference spectrum between the epochs with the highest and lowest continuum level. Although some residual line flux appears in the difference spectrum, this residual is at the 2.2σ level, and may be due the systematic uncertainty in the flux calibration. Figures 2.5b-c show how the 35% variations of the 5260Å continuum bring about less than 9% changes in Hβ. The Hγ light curve (not plotted) is also consistent with being constant, but the larger errors for Hγ (due to the smaller equivalent width and hence larger effects

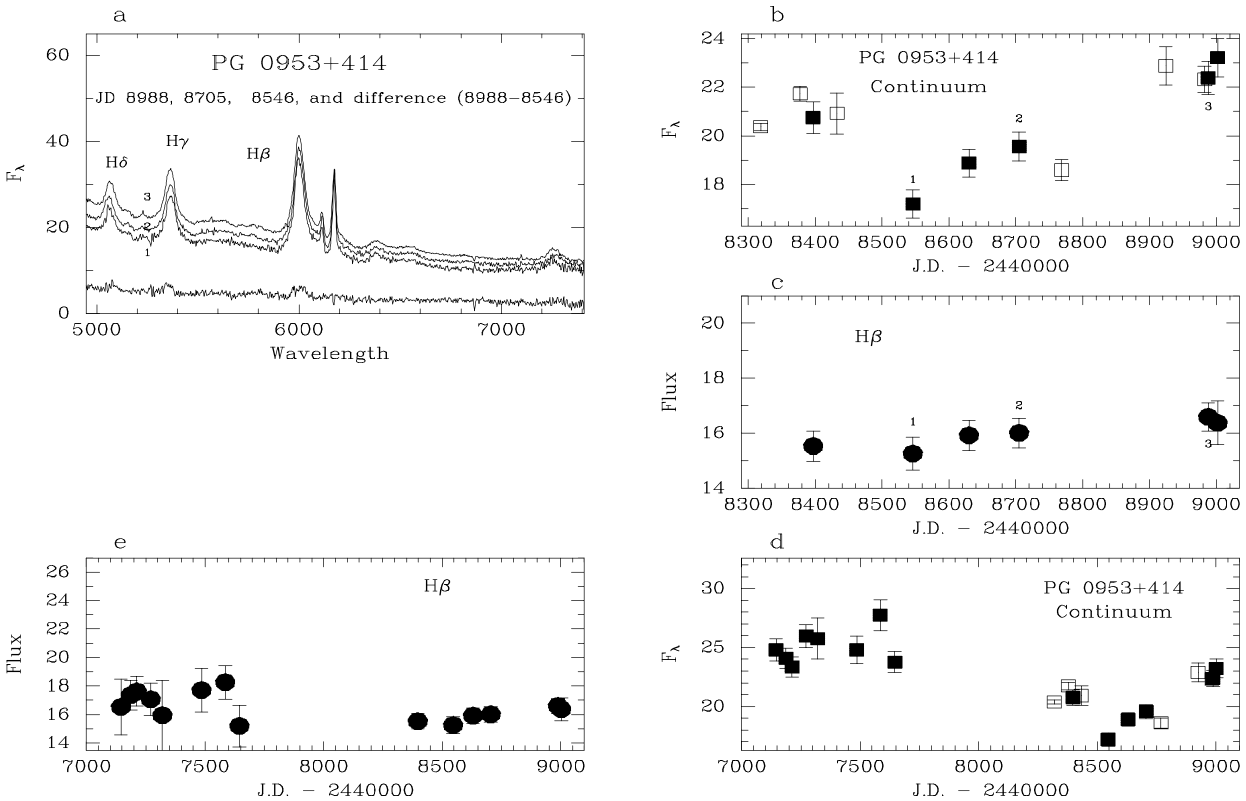

Figure 2.5: Same as Fig. 2.2 for PG 0953+414.

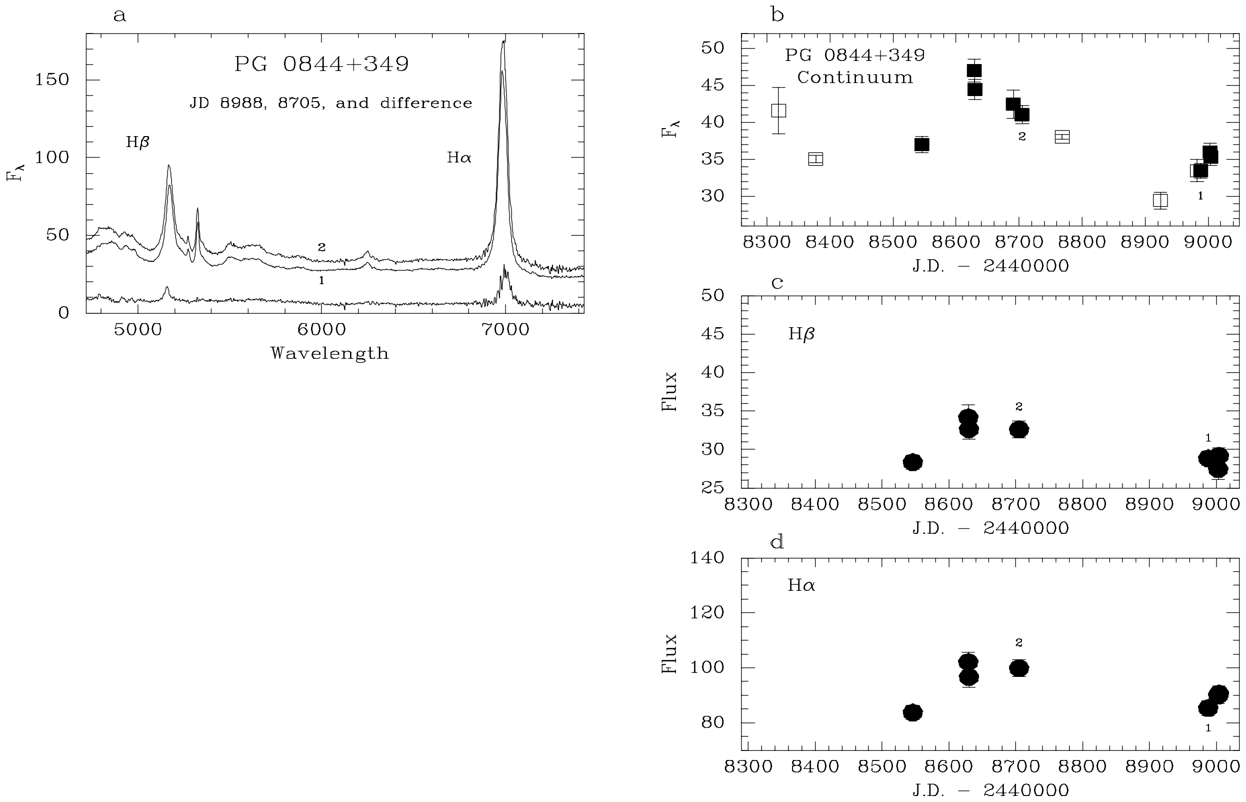

Figure 2.4: Same as Fig. 2.2 for PG 0844+349.

stars.) The Steward and Wise spectral observations alternate in the light curves in Figs. 2.3d-f (3 Wise spectra and 3 Steward spectra), and match very well with each other. Considering also the independent measurement of the same continuum behavior by the Wise photometry (open squares in Fig. 2.3d) which is relative to many stars in the field, there is no doubt as to the reality of the line and continuum variations that are measured.

2.3.3 PG 0844+349

The spectra of this relatively faint ($L_{44} = 4.7$) quasar, two of which are plotted in Figure 2.4a, also show small but significant Balmer-line variations. The light curves in Figs. 2.4b-d again show that the line changes are correlated with the continuum, but have smaller amplitude: 40% variations in the continuum bring about $\sim 15\%$ changes in the lines. The sampling in this case does not allow much to be said about the delay time, except that it is likely to be less than a year.

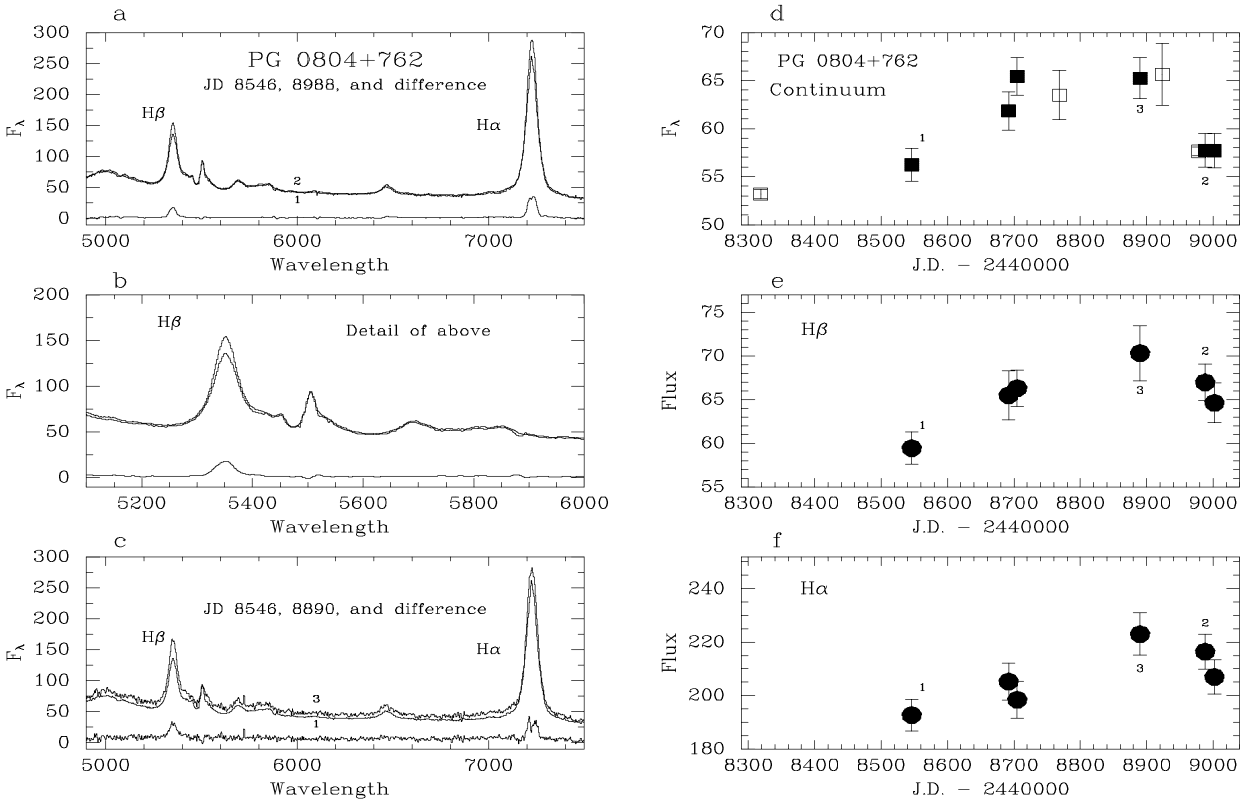

Figure 2.3: Same as Fig. 2.2 for PG 0804+762.

Clear Balmer line variations are detected. There is little or no variation in the strength of the prominent FeII emission features on either side of Hβ. The light curves (Figs. 2.3d-f) are the best sampled among the objects we have observed. The 5240 Å continuum shows a two-year rise and fall of 23%. This variation is mimicked by Hβ and Hα with a similar amplitude. This is the only variable quasar in our sample in which the continuum and line variation amplitudes are comparable. The lines appear to follow the continuum with a lag smaller than the typical sampling interval. The lag is probably less than ~ 200 days. For reference, the optical continuum luminosity of this quasar is ~ 30 times brighter than that of the Seyfert galaxy NGC 5548, where the Balmer line variations lag behind the continuum by a few weeks (Netzer et al. 1990; Peterson et al. 1991; Dietrich et al. 1993).

This type of correlated line and continuum behavior might be suspected as a systematic error arising from a variable comparison star, especially in the absence of forbidden spectral lines with which to test for such an effect. Fortunately, the spectral observations of this quasar used different comparison stars at Wise and at Steward. (The data were intercalibrated by obtaining a simultaneous long-slit exposure of the two comparison

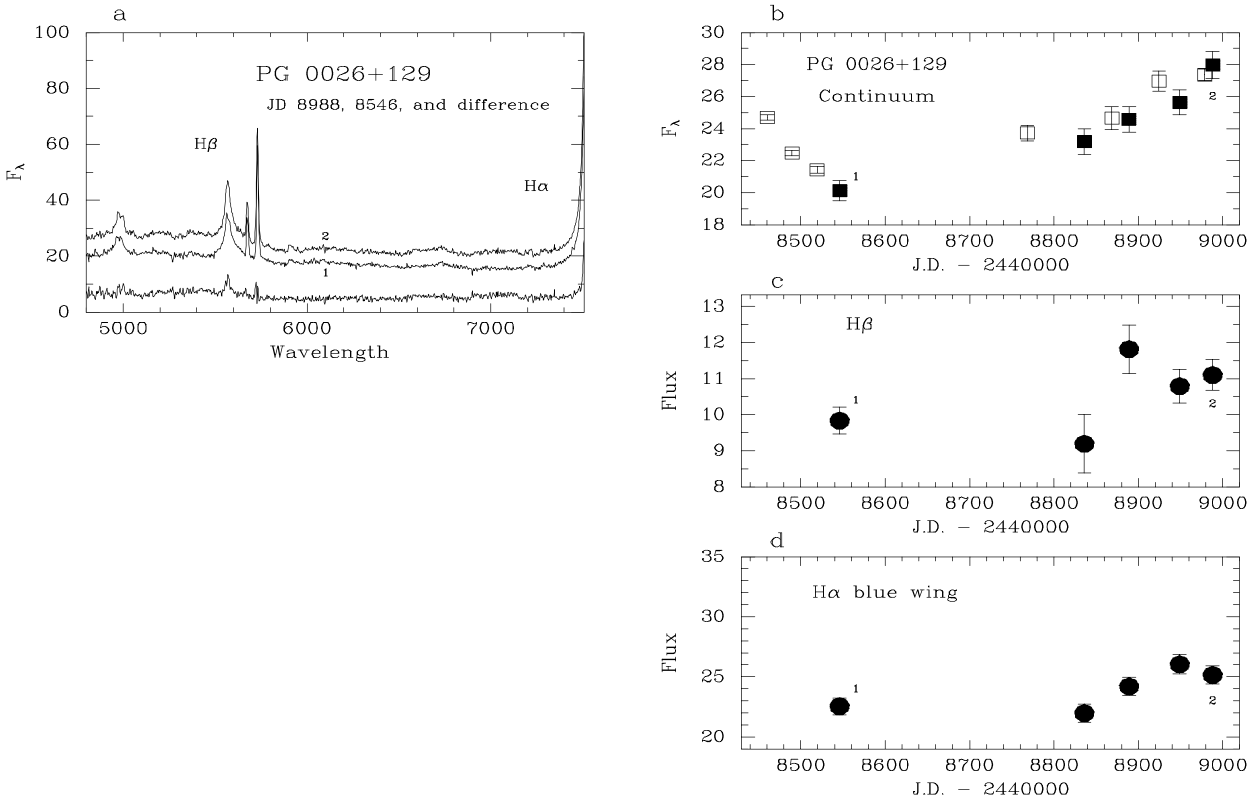

Figure 2.2: Spectra and light-curves for PG 0026+129. Left panel shows spectra at selected epochs, identified in the figure, and their difference spectra. No scaling or offsetting of the spectra has been performed. Objects with variable lines show a residual line component in the difference spectra. Panels on the right show the light curves for the ~ 4800Å continuum and the Balmer lines of each object. The epochs for which spectra are displayed are marked by numerals. Filled symbols are spectrophotometric measurements from Steward and Wise Observatories. Open symbols in the continuum light curves are B-band photometric measurements from Wise Observatory. The latter have been scaled so as to match one photometry point in every object to a spectrophotometric continuum measurement that is close in time. F_λ is in units of 10^{-16} erg s^{-1} cm^{-2} Å^{-1}. Line fluxes are in units of 10^{-14} erg s^{-1} cm^{-2}. See text for additional discussion.

2.3.2 PG 0804+762

Although apparently bright and intrinsically luminous, this quasar has been little studied, probably because the weakness and blending of its forbidden lines makes it impossible to use them for flux calibration. Gondhalekar (1990) compared three IUE spectra taken over a 6-year period, and found a change of 0.26 in both UV continuum and Lα strength between two epochs.

Figures 2.3a-c show spectra from several epochs and their differences for this object.

Table 3: B and R Photometry for Six Quasars

PG 0026+129		
J.D. −2440000	B	R
8460	15.802 ±0.006	15.087 ±0.008
8489	15.912 ±0.012	15.177 ±0.016
8519	15.950 ±0.020	15.154 ±0.036
8768	15.848 ±0.017	15.232 ±0.080
8868	15.818 ±0.035	15.016 ±0.006
8924	15.698 ±0.036	14.967 ±0.015
8978	15.700 ±0.015	...
PG 0804+762		
J.D. −2440000	B	R
8318	14.582 ±0.006	14.037 ±0.008
8768	14.373 ±0.048	13.871 ±0.012
8923	14.362 ±0.051	...
8978	14.496 ±0.014	13.963 ±0.031
PG 0844+349		
J.D. −2440000	B	R
8318	15.101 ±0.003	14.248 ±0.006
8377	15.307 ±0.004	14.392 ±0.033
8768	15.202 ±0.006	14.345 ±0.040
8924	15.493 ±0.005	14.581 ±0.044
8982	15.343 ±0.065	14.467 ±0.086
PG 0953+414		
J.D. −2440000	B	R
8318	15.579 ±0.004	15.203 ±0.005
8377	15.509 ±0.008	15.158 ±0.003
8432	15.577 ±0.030	15.156 ±0.019
8768	15.678 ±0.031	15.223 ±0.013
8924	15.457 ±0.037	15.080 ±0.006
8982	15.466 ±0.044	15.088 ±0.012
PG 1229+204		
J.D. −2440000	B	R
8318	16.093 ±0.007	15.037 ±0.008
8378	16.034 ±0.013	15.006 ±0.017
8432	15.951 ±0.069	15.014 ±0.009
8768	15.671 ±0.009	14.725 ±0.032
8805	15.626 ±0.013	14.711 ±0.011
8985	15.760 ±0.045	14.818 ±0.011
PG 1613+658		
J.D. −2440000	B	R
8411	15.451 ±0.008	14.889 ±0.023
8412	15.435 ±0.007	14.808 ±0.020
8460	15.320 ±0.014	14.767 ±0.007
8489	15.284 ±0.009	14.799 ±0.014
8767	15.065 ±0.022	14.704 ±0.020
8803	15.088 ±0.008	14.639 ±0.008
8867	15.103 ±0.015	14.578 ±0.009
8923	15.011 ±0.011	14.518 ±0.021

Table 2: Line and Continuum Fluxes for Six Quasars

PG 0026+129				
Date (yymmdd)	J.D. −2440000	Continuum (5410-5470Å)	Hβ (5510-5656Å)	Hα (blue wing) (7306-7518Å)
911016	8546	20.1± 0.61	982 ± 37	2253± 68
920801	8836	23.1± 0.78	918 ± 80	2196± 74
920924	8889	24.5± 0.79	1181± 67	2418± 75
921122	8949	25.6± 0.78	1078± 47	2603± 80
930101	8988	27.9± 0.84	1109± 42	2514± 76

PG 0804+762				
Date (yymmdd)	J.D. −2440000	Continuum (5226-5266Å)	Hβ (5268-5476Å)	Hα (6942-7414Å)
911016	8546	56.2± 1.6	5941± 184	19263± 590
920310	8692	61.8± 1.9	6546± 282	20520± 696
920324	8705	65.4± 1.9	6627± 207	19837± 688
920924	8890	65.2± 2.1	7028± 316	22296± 790
930101	8988	57.7± 1.7	6694± 205	21638± 651
930114	9002	57.6± 1.7	6459± 226	20691± 638

PG 0844+349				
Date (yymmdd)	J.D −2440000	Continuum (5050-5080Å)	Hβ (5100-5250Å)	Hα (6850-7122Å)
911016	8546	36.9± 1.1	2833± 89	8369± 258
920107	8629	46.9± 1.5	3416± 164	10203± 346
920108	8630	44.4± 1.3	3262± 128	9661± 364
920309	8691	42.4± 1.9	– –	– –
920324	8705	41.0± 1.2	3259± 107	9981± 303
930101	8988	33.4± 1.0	2884± 83	8531± 257
930115	9003	35.9± 1.2	2741± 133	8990± 285
930116	9004	35.2± 1.0	2916± 105	9058± 281

PG 0953+414				
Date (yymmdd)	J.D. −2440000	Continuum (5240-5280Å)	Hγ (5286-5452Å)	Hβ (5908-6088Å)
910521	8397	20.7± 0.65	763± 57	1552± 55
911016	8546	17.2± 0.57	694± 66	1524± 60
920109	8630	18.8± 0.56	711± 26	1591± 54
920324	8705	19.5± 0.59	714± 34	1600± 53
930101	8988	22.3± 0.67	756± 27	1658± 51
930114	9002	23.2± 0.79	720± 101	1636± 79

PG 1229+204				
Date (yymmdd)	J.D. −2440000	Continuum (5054-5090Å)	Hβ (5096-5246Å)	Hα (6840-7150Å)
910522	8398	20.2± 0.69	1833± 83	6628± 201
920423	8735	32.4± 0.99	2295± 78	7921± 244
930101	8988	26.7± 0.80	2260± 69	8125± 245
930117	9005	35.2± 1.09	2132± 83	8180± 269

PG 1613+658				
Date (yymmdd)	J.D. −2440000	Continuum (5306-5356Å)	Hβ (5362-5712Å)	Hα (blue wing) (7242-7412Å)
910521	8397	29.4± 0.9	2742± 213	4958± 148
910617	8425	32.3± 1.0	2582± 183	4336± 130
910618	8426	33.2± 1.0	2295± 164	4020± 121
911016	8546	34.9± 1.0	2635± 149	4620± 138
920423	8735	37.4± 1.1	2837± 143	4328± 130
920509	8752	39.1± 1.2	2897± 189	4583± 137
920731	8835	41.7± 1.2	2487± 151	3932± 119

Note.- Continuum in units of 10^{-16} erg s^{-1} cm^{-2} Å^{-1}. Line fluxes are in units of 10^{-16} erg s^{-1} cm^{-2}. Wavelength integration limits are in the observer's frame.

variations in the range of 10% to 75%. We present below data for six of these quasars, having the largest variations and best sampled light curves.

Table 2 presents our measurements for the continuum and line fluxes of the six quasars we discuss below. Table 3 lists the B and R-band magnitudes for these six quasars from the CCD photometry at Wise Observatory. The data in Tables 2 and 3 are presented in Figs. 2.2-2.7, together with representative spectra at various epochs for each quasar, and their differences. We discuss each quasar individually below.

2.3.1 PG 0026+129

The strong [OIII] lines of this quasar have made it amenable to previous variability studies relying on these lines for flux calibration. Zheng et al. (1987) reported a factor 2 change in continuum and Hβ strengths over a 10-month period, and Korista (1991) described Hβ line variations of order 15% on time scales of 70 days to 1 year.

Figure 2.2 shows two of our spectra for this quasar, the light curves for the continuum at 5540 Å (observed wavelength) combined with the B-band measurements, and light curves for Hβ and the blue wing of Hα. In this and all other figures in this paper, the spectra are presented as they are produced by our calibration process: no offsetting or scaling of the spectra has been introduced in the plots. The continuum light curve (Fig. 2.2b) shows a decrease in the quasar's brightness during the first observing season, followed by a slow rise in the second year of observations, giving a 40% continuum variation amplitude. The two emission-line light curves (Figs. 2.2c and 2.2d) show small but significant changes that clearly go in the same sense as the continuum. The continuum and line changes are also apparent in Fig. 2.2a, in the difference spectrum between two epochs. Ignoring the noisier Hβ measurements in the light curves, Hβ and the $H\alpha$ blue wing varied by 10% and 15%, respectively, i.e. 3-4 times less than the optical continuum. Our results confirm the line variability reported by Zheng et al. (1987) and Korista (1991) for this object, and show that these changes are, in fact, responses to continuum variations. The delay in the line response appears to be less than one year.

on the same night as the R photometry to the measured rest-frame 4800Å flux, from the spectroscopic observation. This scaling was applied to all B measurements of a given quasar and resulted in excellent agreement between the spectroscopic and the photometric light curves at other epochs. (In other words, the B-band and the 4800Å continuum have similar relative variation amplitudes.)

2.3 Results

In this section we present photometric and spectrophotometric data for our sample from 1991 March to 1993 January. Following a brief description of the behavior of the sample as a whole, we present continuum and emission-line light curves for six variable quasars for which the data are presently of the best quality in terms of S/N and temporal sampling. A detailed analysis of the continuum variation properties will be presented elsewhere.

Table 1 lists for the quasars in our sample the average F_λ(4800Å) flux we measure for each object (wavelength in the object's rest-frame), the 1000-10,000 Å luminosity (assuming $H_0 = 75$ km sec^{-1}Mpc^{-1}, $q_0 = 0.5$, and that the spectral shape can be described by a power-law of slope -0.5 in F_ν), the number of separate epochs it was successfully observed spectroscopically ("separate" meaning separated by more than one day), the temporal baseline, and the continuum variation amplitude, defined as $F_{\rm max}/F_{\rm min} - 1$ at 4800Å, during this period. Of the 28 quasars in our sample, 22 have been observed spectroscopically more than once. Among these 22 objects, the number of spectrophotometry epochs per object is 2 to 9, with a median of 5. The temporal baseline is typically 1 to 2 years. Table 1 also shows that, in terms of the distribution of variation amplitudes over $1 - 2$ years, the sample has behaved largely as found by Keel and Allan (1991). Eight quasars show little ($< 5\%$) or no continuum and line variations, with spectra separated by a year sometimes matching to better than 1%. The comparison star chosen for one of these objects, PG 1211+143 (the 14th-mag star $2'$ south-west of the quasar), turned out to be variable. Fortunately, the photometry data for this object show that the continuum variations in the quasar were $< 5\%$. The remaining 14 quasars underwent continuum

provides a robust check on the continuum behavior measured by the spectroscopy, since the quasar brightness is measured relative to a number of stars in the field, rather than just one (after the stars have been tested for variability against each other). The differential photometry is also safe from other problems that could potentially affect the spectroscopy, such as differential atmospheric refraction at high air mass.

The photometric observations are part of a large scale monitoring program that will be described elsewhere (Netzer et al. 1993, in preparation). Below is a brief summary of the technical details necessary for the current work. The observations were carried out with an RCA 512×320 thinned CCD in direct imaging mode, at the f/7 focus of the Wise 1m telescope. The pixel scale was 0.88 arcsec pixel^{-1}. Exposures of 3 minutes in B and 2 minutes in R were obtained for every quasar. The images were bias-subtracted and flat-fielded and the DAOPHOT package was used for measuring the stellar and quasar fluxes. Three to six stars in each frame were chosen as local standards, after verifying that they are not variable. The fluxes of the local standards were transferred to an absolute scale using photometric standards. The B and R magnitudes of the quasars were obtained by solving for the linear relation between the instrumental and known magnitudes of the reference stars. Typical 1σ uncertainties for the six objects under study are 0.02-0.03 mag.

In order to combine our broad-band and spectroscopic measurements of each quasar into one continuum light curve, we have carried out the following cross-calibration. For each of the six quasars discussed below, we have numerically integrated over the spectrum of the local comparison star, using the R filter transmission curve and the CCD response curve. The resulting magnitude was compared with the magnitude of the comparison star measured from the R-band CCD photometry, and showed good agreement (-0.09 to +0.11 mag with a mean deviation of 0.06 mag.). For every quasar we then found the pair of photometric and spectroscopic observations that are closest in time (10 days or less in all cases) and verified, using the integration over the R band, that the quasar did not vary between the observations. Finally, we scaled the B photometry that was taken

and demonstrates the good reproducibility of the method. We also find excellent agreement between spectra taken at Wise and at Steward Observatories when the observations are of non-variable objects or are close in time. An independent check of the continuum variations of the quasars measured from the spectrophotometry, and of the the assumption that the comparison stars do not vary, comes from contemporaneous CCD photometry of the sample (see below).

For every quasar, we examined the best S/N spectra and chose line-free spectral bands suitable for setting the continuum underlying the emission lines, and the wavelength limits for integrating the lines. The continuum and line fluxes were then measured automatically for all epochs by calculating the mean flux in the continuum bands and summing the flux above a straight line in F_λ between the continuum bands straddling the emission line. The error in the line flux was calculated by propagating the error in the setting of the continuum levels, determined from the standard deviation of the mean in the continuum bands. To the errors in the line and continuum measurements, we added in quadrature an error of 3% corresponding to our estimate for the flux calibration uncertainty of an individual spectrum. In some objects, Hα is redshifted to the edge of the spectral range, making it difficult to determine the continuum level on the red side of the line. In some of these quasars we measured $H\alpha$ by setting only the continuum on the blue side of the line, and extending it to the red at constant F_λ, if this seemed justified based on the continuum shape in spectra having longer wavelength coverage. In some cases, only the blue wing of Hα was measured. Further details on the measurements of individual objects are given in § 2.3.

2.2.3 Broad-Band Photometry

In conjunction with the spectrophotometry described above, we have carried out broad-band B and R differential CCD photometry of the sample at the Wise Observatory 1m telescope. Since the continuum emission dominates the signal in the broad bands, these data supply us with additional epochs for the continuum flux. The photometry also

to obtain calibrated spectra of each quasar for all epochs. The calibrated spectra of the comparison stars were determined from measurements of spectrophotometric standards on nights that were photometric. The absolute calibration of a set of spectra for a given quasar is therefore accurate to $5-15\%$, depending on the number of spectrophotometric calibrations that were obtained for the comparison. The differential spectrophotometric accuracy relative to the comparison star, which is our main concern in this program, is much better.

From comparison of the different-epoch spectra of the least variable quasars, we estimate the relative flux calibration error to be $\sim 3\%$. Figure 2.1 shows spectra for one of these non-variable quasars, PG 1404+226, from two epochs separated by ten months,

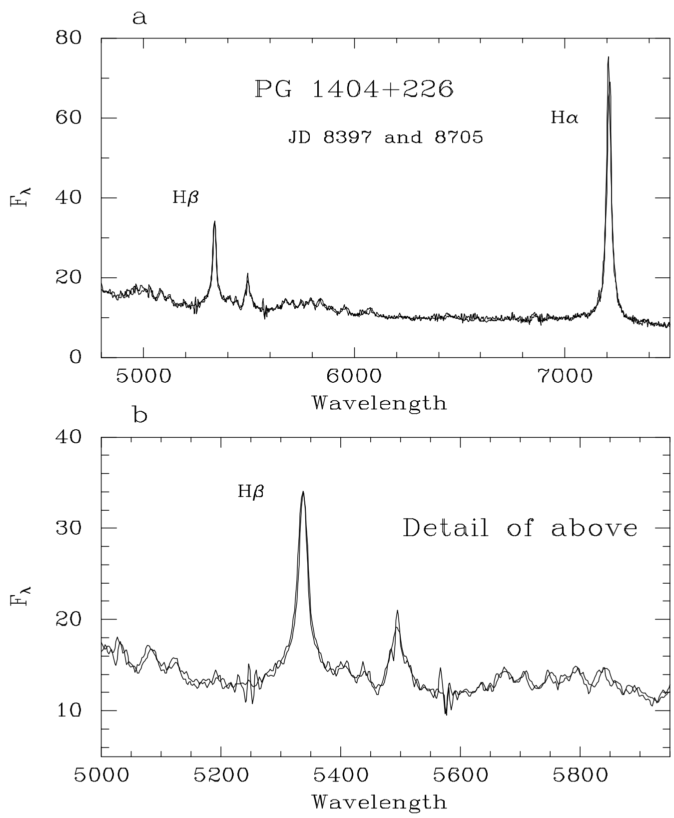

Figure 2.1: Superposed spectra of the quasar PG 1404+226 at two epochs separated by 10 months. This is one of several quasars in the sample that was not observed to vary, and demonstrates the accuracy and repeatability of the relative spectrophotometry. The features at 5250Å and 5570Å are residuals from night-sky lines. F_λ is in units of 10^{-16} erg s^{-1} cm^{-2} Å^{-1}.

the lowest redshift Seyferts, always redshifted into the complex atmospheric absorption bands beginning at 6900Å. The simultaneously obtained spectrum of the comparison star under exactly the same conditions allows a near-perfect correction of this absorption and hence an accurate measurement of the $H\alpha$ line.

Two consecutive exposures of every accessible quasar/star pair were usually obtained in every run. Exposure times were typically 15 min per exposure at Steward and 1hr at Wise. The spectroscopic data were reduced using standard IRAF routines. Lamp flats taken adjacent to every exposure were used to correct for pixel-to-pixel variations in sensitivity (and also sharp wavelength-dependent sensitivity changes in the Wise FOSC). Dome or twilight flats were used to correct the images for changes in the illumination along the slit (important mainly in the Steward spectra). The spectra of each quasar and its comparison star were extracted in a standard way and were wavelength-calibrated by using He-Ar arc spectra extracted from arc exposures taken adjacent to every object exposure.

The quasar/star flux ratios between consecutive exposures were compared to test for any systematic errors in the observation (e.g. slit angle errors, guiding or positioning errors, loss of light due to differential atmospheric refraction). The ratios almost always reproduced to 1-2% at all wavelengths. The few epochs where the ratios between exposures differed by more than 5% were discarded. The quasar and star spectra from the consecutive exposures were co-added to improve S/N, and the resultant quasar spectrum divided by an absorption-line-interpolated and smoothed version of the co-added star spectrum. (The spectral region of the star with atmospheric absorption bands was *not* smoothed, in order for the division to properly remove these absorptions from the quasar spectrum.) The wide slits used to ensure accurate photometry caused some degradation of the wavelength calibration. Small shifts in wavelength were made in the quasar/star ratios to bring all epochs of a quasar to a common wavelength scale, judging by the prominent emission features (usually the [OIII]λ5007 line and the $H\alpha$ peak). The quasar/star ratios for all epochs were multiplied by a smoothed flux-calibrated spectrum of the comparison star,

2.2.2 Spectrophotometric Observations and Reduction

The spectroscopic observations were carried out at the Steward Observatory 2.3m telescope and at the Wise Observatory 1m telescope. The Steward observations used the Boller and Chivens spectrograph with a $4.5''$-wide slit, a 300 line/mm grating and a 800×800 TI CCD, giving a dispersion of 3.7Å per pixel, and a spectral resolution of $\sim$ 8Å, covering the range from 4600Å to 7500Å. In 1992 September and 1993 January a 1200×800 Loral CCD was used, with similar dispersion and an increased (4000Å to 8300Å) spectral range. The Wise spectroscopy was done with the Faint Object Spectrograph Camera (FOSC). This is an all-transmission-optics instrument similar to the European Southern Observatory's EFOSC, in which grisms can be swung into the collimated beam to alternate between imaging and spectroscopy of an object. The FOSC has a 1024×1024 TI CCD detector. We used a $15''$-wide slit and a 300 line/mm grism, which gave a dispersion of 4.5Å per pixel and a spectral resolution of $\sim$ 10Å. The optics of the system restrict the usable spectral range to $\sim$ 4400Å – 7900Å.

For every quasar, the spectrograph was rotated to the appropriate position angle to simultaneously include a nearby (<4 arcminute) field star within the slit, which served as a standard. This technique was shown by Maoz et al. (1989) to yield a 1σ photometric error of 3% when used for Seyfert galaxies on the Wise 1m telescope. The high photometric accuracy obtainable with this technique is especially important in quasar monitoring since, as shown by Keel and Allan (1991) and confirmed by our results below, typical quasar variation amplitudes are only a few tenths of a magnitude. As we shall see, the emission line variations are even smaller. Apart from the high photometric accuracy that is obtained, this calibration method has several important advantages over other methods used in AGN monitoring. Spectrophotometric data can be obtained even during relatively poor weather, thus decreasing the likelihood of gaps in the sampling. The narrow forbidden lines which are often used for flux calibration in Seyfert monitoring programs are frequently weak, absent, or blended in quasars, and could therefore not be used. The $H\alpha$ line (usually the second strongest emission line in AGNs, after Lyα) is, except for

$H\beta$ line within our observable spectral range ($4500 - 7500$Å). Based on the original B magnitudes of Schmidt and Green (1983), we required $B < 16$, to provide adequate S/N in brief exposures, and $M_B < -23$, which is a commonly-used defining border between Seyfert galaxies and quasars. One quasar (PG 1151+117) was dropped from the sample when the first observations in 1991 May showed that it was considerably fainter than expected. A final criterion was the presence of a suitably bright field star within 3.5 arcminutes of the quasar, which served as a comparison star for the quasar (see below). Our sample consists of 28 quasars satisfying these criteria, listed in Table 1.

Table 1: The Sample

PG-Object	B	z	$-M_B$	F_λ(4800Å)[a]	L_{44}[b]	N_{spec}[c]	Δt_{max}(days)	$F_{max}/F_{min} - 1$
0026+129	15.0	0.142	24.8	2.4	16.2	5	442	0.40
0052+252	15.4	0.155	24.5	2.5	20.8	6	465	0.68
0804+762	15.2	0.100	23.7	5.9	18.8	6	456	0.25
0844+349	14.0	0.064	24.0	3.8	4.7	6	458	0.62
0953+414	15.1	0.239	25.3	2.0	44.1	6	605	0.41
1048+343	15.8	0.167	23.4	0.7	6.7	1		
1100+772	15.9	0.313	25.6	1.1	44.2	2	253	0.25
1202+281	15.6	0.165	24.3	0.8	7.5	3	353	0.67
1211+143	14.6	0.085	23.9	7.6	17.0	5	612	0.00
1226+023	12.8	0.158	27.1	30.5	259.8	9	651	0.22
1229+204	14.7	0.064	23.3	2.8	3.4	4	607	0.75
1307+086	15.3	0.155	24.5	2.5	20.4	3	354	0.20
1309+355	15.5	0.184	24.6	2.6	31.0	2	337	0.05
1322+659	15.9	0.168	24.1	1.4	13.7	2	311	0.00
1351+640	15.4	0.087	23.3	5.8	13.8	5	591	0.17
1354+213	15.9	0.300	25.6					
1402+261	15.6	0.164	24.5	2.0	18.5	1		
1404+226	15.8	0.098	23.1	1.2	3.6	2	308	0.00
1411+442	15.0	0.089	23.7	4.4	10.9	3	325	0.00
1415+452	15.7	0.114	23.5	1.6	6.7	1		
1426+015	14.9	0.086	23.7	5.0	11.5	4	374	0.05
1444+407	16.0	0.267	23.3					
1512+370	16.0	0.371	25.9	0.5	30.1	2	352	0.00
1613+658	15.4	0.129	24.1	3.7	20.2	6	438	0.55
1617+175	15.5	0.114	23.7	1.5	6.3	5	373	0.31
1700+519	15.4	0.292	25.9	3.0	102.6	2	123	0.00
1704+608	15.9	0.371	26.0	2.2	132.4	1		
2130+099	14.6	0.061	23.2	4.8	5.4	8	486	0.31

[a] Mean measured flux density at 4800Å (wavelength in the quasar rest-frame), in units of 10^{-15} erg s^{-1} cm^{-2} Å^{-1}.
[b] Luminosity between $0.1 - 1\mu m$ in units of 10^{44} erg s^{-1}, based on F_λ(4800Å) given above, and assuming $H_0 = 75$ km s^{-1}Mpc^{-1}, $q_0 = 0.5$, and a power-law continuum spectral index $\alpha_\nu = -0.5$.
[c] Number of separate spectral epochs.

redshifted into atmospheric absorption bands in low-redshift quasars.

In § 2.2, we define our quasar sample and describe our observations. In § 2.3 we present our results for some of the quasars in the sample. We discuss and summarize these results in § 2.4.

2.2 Sample and Observations

2.2.1 Sample Definition

The Palomar-Green (PG) sample of quasars (Schmidt and Green 1983) is well-suited for quasar emission-line monitoring. The brightness of the PG quasars ($B < 16$) enables spectra to be obtained for about 4–10 quasars a night on a small to medium-sized telescope. The low redshift of most of the PG quasars keeps the Balmer series in the optical range, and cosmological time dilation does not significantly lengthen the various timescales. The PG quasars form a complete $U - B$ color-selected sample whose spectral properties have been well studied (Neugebauer et al. 1987; Kellermann et al. 1990; Berriman et al. 1990; Boroson and Green 1992). Variability characteristics can therefore be tested for correlations with the other properties of the quasars. Another advantage is that the continuum variability properties of the PG sample have been studied (Keel and Allan 1991), allowing an estimate of the number of quasars that needed to be monitored in order to detect moderate variations in some of the objects. Keel and Allan found from broad-band monitoring of most of the PG quasars over a period of 3.5 years that 30% of them varied by 0.2 to 1 mag in the B and V bands. We therefore expected that by monitoring about 30 quasars for 1-2 years we would detect continuum variations potentially large enough to drive emission-line variations in 5-10 objects. This expectation has been borne out by our results, described below.

To cull the PG quasar sample to about 30 objects, we made cuts in declination, redshift, apparent magnitude, and absolute magnitude. We included only quasars with northern declination so as to be able to monitor them for longer intervals from northern hemisphere telescopes. We accepted only quasars with redshifts less than 0.4, keeping the

to apparently bright objects, i.e. Seyfert galaxies. The one exception is the bright quasar 3C 273, which has been extensively studied by IUE (O'Brien and Harries 1991; Ulrich et al. 1993). The UV observations show that the Lyα line in 3C 273 varies much less than the UV continuum, in contrast to Seyfert galaxies, where the amplitudes are comparable. The low variation amplitude of the lines observed with IUE make the determination of the line-continuum lag difficult. O'Brien and Harries (1991) and Koratkar and Gaskell (1991) reported lags of 118 and 74 days, respectively, while Ulrich et al. (1988, 1993) argue that the line variations are marginally significant and so a lag cannot be determined. Even for this bright object, accurate ground-based optical spectrophotometry has been hampered by the fact that the narrow forbidden lines (which are often used for flux calibration in AGN monitoring programs) are weak and are blended with strong broad FeII emission (Zheng et al. 1987).

Because of the small number of quasars where line monitoring has been attempted and the difficulties outlined above, the picture is presently unclear regarding the basic questions of quasar emission-line variability: Do quasar emission lines respond to continuum changes, as seen in Seyfert galaxies? What is the relative amplitude of the response? What is the lag of the response, reflecting the light-travel time across the BLR? Do quasar BLR sizes scale with AGN luminosity, and lie on a continuous relation from the faintest Seyferts to the brightest quasars? The answers to these questions could provide valuable clues toward the understanding of the nature and evolution of AGNs.

In this paper we present results from an observing program designed to address the above questions. Our program deals with the difficulties of quasar monitoring in a number of novel ways. We have monitored a large and well-defined sample of UV-excess quasars with a range of luminosities, so that our results have statistical value. We use a relative flux-calibration method that is highly accurate even during non-photometric weather without depending on the presence of narrow forbidden lines in the quasar spectrum. The method also allows accurate measurement of the Hα emission-line, which is difficult to calibrate (there are no strong forbidden lines in this spectral region), and which is usually

as predicted by photoionization models. Only recently has a full application of the line variability mapping technique (also referred to as reverberation- and echo-mapping) been successfully carried out by several groups for a number of Seyfert 1 galaxies (Maoz et al. 1990, 1991; Netzer et al. 1990; Clavel et al. 1991; Peterson et al. 1991). The emission line response times measured by these studies have shown that Seyfert galaxies have BLRs with sizes of several light-days to light-weeks. These sizes are an order of magnitude smaller than originally predicted by photoionization models, and have led to a revision of the models and to new insight into the physical processes in the BLR gas. A recent review of the results of these observational campaigns is given by Peterson (1993).

While progress has been made in studying the emission-line variability of the *low-luminosity* end of the AGN phenomenon, this is not the case for the *high-luminosity* end, the quasars. Relatively little work has been done to map the broad-line regions of quasars. Old photoionization models predicted a BLR size for quasars of several lt-years (and this expected long timescale played a role in discouraging attempts at quasar line monitoring). If one naively scales down the old prediction, following the Seyfert echo-mapping results, BLRs of several lt-months are implied for quasars. Indeed, there have been reports of correlated line and continuum variations in quasars, with delays smaller than the sampling intervals (*e.g.* Zheng et al. 1987; Perez, Penston, & Moles 1989; Gondhalekar 1990; O'Brien and Harries 1991; Korista 1991; Hooimeyer et al. 1992). The sampling intervals have been of order months to 10 years, and the measurements often have involved only two or three epochs per object. Some of these results are controversial due to uncertainty regarding the accuracy of the photometric calibration. On the other hand, some observations indicate continuum variations with little or no line changes (*e.g.* Ulrich et al. 1988; Jackson et al. 1992, Ulrich, Courvoisier, & Wamsteker 1993).

The main limitation to the study of quasars has been their faintness. Much of our knowledge on AGN emission-line variability comes from the IUE satellite, for which most quasars are too faint. Because of the large demand on telescope time required by monitoring campaigns, ground-based studies have been limited to small telescopes and therefore

Abstract

We have monitored spectrophotometrically a subsample (28) of the Palomar-Green Bright Quasar Sample for two years in order to test for correlations between continuum and emission-line variations and to determine the timescales relevant to mapping the broad-line regions of high-luminosity AGNs. Half of the quasars showed optical continuum variations with amplitudes in the range 20-75%. The rise and fall time for the continuum variations is typically 0.5-2 years. In most of the objects with continuum variations, we detect correlated variations in the broad $H\alpha$ and $H\beta$ emission lines. The amplitude of the line variations is usually 2-4 times smaller than the optical continuum fluctuations. We present light curves and analyse spectra for six of the variable quasars with 1000-10000Å luminosity in the range of 0.3–4$\times10^{45}$ erg s^{-1}. In four of these objects the lines respond to the continuum variations with a lag that is smaller than or comparable to our typical sampling interval (a few months). Although continued monitoring is required to confirm these results and increase their accuracy, the present evidence indicates that quasars with the above luminosities have broad-line regions smaller than about 1 lt-year. Two of the quasars monitored show no detectable line variations despite relatively large-amplitude continuum changes. This could be a stronger manifestation of the low-amplitude line-response phenomenon we observe in the other quasars.

Subject Headings: quasars: individual – quasars: emission lines – quasars: variability

2.1 Introduction

A great deal of progress has been made in recent years in the study of active galactic nuclei (AGNs) as the result of several spectroscopic AGN monitoring projects designed to map the emission line regions of these objects. A time delay between the continuum and broad emission line light curves can be interpreted as the effect of the light travel time from the central source to the line-emitting gas, and is directly related to the size and geometry of the broad line region (BLR). Observations carried out over the past decade established that the emission lines in Seyfert galaxies respond to variations in the continuum fluxes,

Chapter 2

How Fast Do Quasar Emission Lines Vary? First Results from a Program to Monitor the Balmer Lines of the Palomar-Green Quasars

Dan Maoz[1,4,5], Paul S. Smith[2], Buell T. Jannuzi[1,4], Shai Kaspi[3], and Hagai Netzer[3]

[1] Institute for Advanced Study, Princeton, NJ, 08540

[2] Steward Observatory, University of Arizona, Tucson, AZ 85721

[3] School of Physics and Astronomy and the Wise Observatory,
Raymond and Beverly Sackler Faculty of Exact Sciences
Tel-Aviv University, Tel-Aviv 69978, Israel

[4] Guest Observer, Steward Observatory

[5] Guest Observer, Wise Observatory

Published in *The Astrophysical Journal*, **421**, pp. 34 – 45, 1994 Jan 20.

is very bad. Observations by Sitko (1990), who monitored the quasar GQ Coma with IUE, suffer from bad flux calibration and many spectra with low S/N. He found a BLR size of 50–100 light-days with the DCF method. Pérez, Penston, and Moles (1989), Jacson et al. (1992), and Korista (1991), have reported monitoring of quasars. They were all only for a period of about a year, with sampling every few months. The change in the broad lines was checked by comparing their flux to the flux of $[OIII]$ lines which are narrow and not supposed to vary. The authors reported line variations on time scales of a few months, but because of the short monitoring time the results are not sufficient for more specific conclusions.

The purpose of the Palomar-Green (PG) quasars monitoring project, which is described in this work, is to fill the gap between Seyfert 1s and quasars, regarding line monitoring, and to answer some open questions about the BLR in quasars. The project and preliminary results will be described in chapter 2 (which is the paper Maoz et. al. 1994, that was published in the Astrophysical Jornal). Chapter 3 describes further analysis on the same data set.

given in Edelson and Malkan (1987) who also report about 45 AGNs which were observed by *IRAS*. They found that "normal" quasars varied with amplitude less than 15% in 6 months at the IR range, but BL-Lacs and OVVs changed much more in that period.

Those studies and others show that the continuum flux in quasars is variable. There is strong evidence that the amplitude of the variability is luminosity dependent. Also, the variability of the continuum is wavelength dependent. At longer wavelengths, the variability time scale is longer and the relative changes are small. Although the continuum behavior of quasars is well studied, the emission-lines variability is not well known. Only a few studies were made, and the correlation between the continuum and the emission-lines is not really known.

The most studied quasar is 3C 273, which is very bright. The multi-wavelength review of its properties is given in Courvoisier et al. (1990). There are Many observation with *IUE* from 1978 to 1989, that are summarized by O'Brian and Harris (1991), who reported also on a monitoring program with a good time resolution (every two weeks) for about 950 days. Together with all the previous years results they found a cross-correlation size of 74 ± 33 days. This is the only quasar which has a good enough data set to obtain a reliable CCF.

There are some more attempts to monitor quasars spectrophotometrically, but they all suffer from bad temporal sampling or bad flux calibration, which result in insufficient data for determining the BLR geometry. Zheng and Burbidge (1986), Zheng et al. (1987), and Zheng (1988), reported a monitoring program of about 30 quasars with the Lick Observatory 3 m telescope for a few years, with about one sampling in a year of each quasar. They found that the emission-line flux changed with response to the continuum changes, but because of the bad time resolution only an upper limit of about 1 light-year for the BLR size was deduced by those authors. Gondhalekar et al. (1986), and Gondhalekar (1990) reviewed observations done on quasars with *IUE*. They found that the continuum and line fluxes changed and deduced a BLR size of 0.01–2 light-years, but their findings are very controversial since the absolute flux calibrations of those observation

is strong evidence that the UV and optical continua vary together with no detectable phase difference, the variable parts of the strong, broad emission-lines are found to arise much closer to the central source than previously supposed, and the BLR shows strong evidence for radial ionization stratification. Thus, monitoring projects lead to a better understanding of Seyfert galaxies and changed our view about the inner regions of AGNs.

While many Seyfert galaxies were studied for variability, very few such studies were carried out on the more luminosity quasars. Although quasars are more energetic than Seyferts, they are fainter because of their large distances. This is the main reason for the need of more advanced technologies and telescopes to obtain good spectra and to apply reverberation techniques to such objects.

The long-term continuum variability of quasars (years time-scale) has been known for some time. Usher (1978) compared 820 objects on photometric plates taken 10 years earlier with new observations, and found that the luminosity of about 170 objects have changed. 70% of those objects were found by him to be quasars. Grandi and Tifft (1974) reviewed data from previous observations on about 100 quasars (from many different sources) and found that 68% varied with amplitude less than 0.5 magnitude, and 9% varied with amplitude ~ 2 magnitude. Zamorani et al. (1984) presented results of monitoring the continuum X-ray flux of quasars with the Einstein Observatory and found that on time-scales of hours there are no changes, few varied on time scales of days, and in time scales of months 9 out of 12 have varied by factors of 2 or less. The UV continuum of 81 quasars, observed with the *IUE*, was reviewed by O'Brian, Gondhalekar, and Wilson (1988). The UV continuum become steeper at shorter wavelengths. Those authors did not find continuum variations on time scales of days but on weeks and months time scales most of the objects varied, by 1 or less magnitude. There is tendency for the varying amplitude to become smaller for more luminous objects. Curri and Wisniewski (1985) monitored the continuum of 7 quasars for three years. They did not find change in the IR continuum (above 1 μm), but the optical continuum changed by about 0.5–1.5 magnitude in a year. A review of the work that was done on continuum variability of quasars is

function which was in agreement with a BLR geometries of spherical shell or a thin disk viewed nearly edge on, with ratio of outer to inner radii of order of 10 ,and with inner radius of order several light-days (Maoz et al. 1991).

Fairall 9 was one of the most luminous Seyfert galaxies at the time of its discovery (Fairall 1977), but since then it has shown a steady decline in both the optical and the UV. It was observe with IUE on more then 50 epochs in 10 years. During that time the continuum of the object declined gradually by a factor of 33. Although this simple behavior and the poor sampling intervals, the huge factor of luminosity change enabled to determine a BLR size of 155 ± 45 light-days for the strong UV lines (Clavel, Wamsteker, and Glass 1989).

Other Seyfert 1 galaxies that were studied in this way are: [1] Mrk 279, in which the Wise Observatory monitoring project in 1988, found this object to have a cross-correlation size of 12 ± 3 light-days (Maoz et al. 1990). [2] Akn 120 was studied by many in the last decade, cross-correlation techniques applied to the data yield size of ~ 30 light-days (Gaskell and Peterson 1987; Peterson and Cota 1987; Alloin et al. 1987). [3] NGC 1566 has been studied by Alloin et al. (1985, 1986) who concluded that the BLR size is less than ~ 20 light-days. [4] The light-curves of the broad components of $L\alpha$ and $CIV\lambda1549$ of the Seyfert 3C 390.3 were cross-correlated with the continuum light-curve by Clavel and Wamsteker (1987) to give a lag of ~ 45 and ~ 25 days, respectively. Several other major studies of individual Seyfert 1 galaxies have been published, see Peterson 1988, 1993 for a review. Also, there are other studies of many Seyfert galaxies which did not show variability during the time of monitoring.

All the above studies produced general and important results concerning Seyfert galaxies. It was found that any change in the continuum flux, produces a change in the broad emission-lines. The typical lag was of order of light-days to light-weeks, indicating a BLR size smaller by an order of magnitude than was predicted by old photoionization models. This led to a revision of the old model to fit the new observational results (Peterson 1993). The monitoring studies have more results than just to measure the BLR geometry: There

1.3 Previous Work on BLR Mapping

Several monitoring project, to determine the continuum and line-light-curves of AGNs, were carried out in the past decade in order to find the transfer function and the BLR size. Most projects concentrated on Seyfert galaxies, at the lower luminosity end of the AGN phenomenon, because they are brighter and tend to vary on shorter time-scales than quasars. One of the more extensive effort was devoted to the Seyfert 1 galaxy NGC 5548. This object was monitored by many observers at many wavelength, since 1988, with a high temporal resolution. This was done by the *International AGN Watch*, using HST, IUE , and ground-based telescopes. Cross-correlation results were obtained for 11 emission-lines, with short lags: from 2 to 22 days (with an exception of cross-correlation size of $34 - 72$ days for $MgII\lambda2798$). When put together, they show a distinct pattern of increasing lag with decreasing ionization level, therefore providing evidence for radial ionization stratification of the BLR. A review of this work is given in Peterson 1993.

Another Seyfert 1 galaxy which was extensively and widely studied is NGC 4151. This is a very bright ($\sim 10 - 11$ magnitude), and fast varying object, that can be observed very easily with medium size telescopes. Works of Antonucci and Cohen (1983), and Peterson and Cota (1988) in the optical range, each for a 14-month period with moderate resolution (about 1 month), resulted in a cross-correlation size of about 6 days with uncertainty of factor 2. Also, a collaboration of European astronomers has produce a set of low dispersion UV spectra at more than 125 epochs with the IUE spacecraft, since it was lunched until mid 1990. This project which is reviewed in Ulrich et al. 1991, resulted with a BLR size of about one light week but since the temporal resolution here is also about 1 month the error is quite large. From the above works it became clear that the BLR size and the variability time is less than the temporal resolution. This led to a better study of NGC 4151 with a very high resolution in 1988 at the Wise Observatory. The object was observed for 67 nights during a 216 days period, i.e., mean of one spectra every three days. From this high quality data-set a cross-correlation size of 9 ± 2 was found for the Balmer lines. Also, this set is the only one that eq. 1.6 was used on it to find a transfer

where N is the number of points used in the sum for the lag τ, σ_C and σ_L are the rms of the light-curves, and the two light-curves have zero means. τ is an arbitrary temporal shift between the two data sets. The lag is the value of τ which maximizes the correlation coefficient between the two series. To carry out this calculation the data points need to be evenly spaced, and for a given $C(t)$, $L(t+\tau)$ need to be measured. Also, the time base of the light-curves need to be large and the object observed need to vary in this time in order to get meaningful results. Those conditions are very hard to achieved with astronomical data sets because of the nature of astronomical observations. Bad weather, and period during which the objects cannot be observed, put many gaps in the light-curves, as well as the fact that no one can anticipate if an AGN will vary or not.

One way to overcome those problems, one option is to interpolate the light-curves. Gaskell and Spark (1986) interpolated between real observational points in the light-curves, and resampled the interpolated light-curves at regular intervals. They also extrapolated one light-curve at a constant level at its ends to avoid discarding data when calculating the F_{CCF} at larger lags. To reduce the effects of adding many interpolated points, only one time series can be interpolated and the cross-correlation is performed using the *real* data points from the other series. A drawback of this method is the need to guess the light-curve behavior between the observed points. Another difficulty may arise if there are correlated errors between the two light-curves, since it is common to measure the continuum flux and the emission-line flux from the same spectrum. Such errors will introduce an artificial correlation at lag 0, hence, corrupting the CCF. A way that partly avoids those problems is the discrete correlation function (DCF) method (Edelson and Krolik 1988). This method uses only observed data points, thus avoiding interpolation (it uses only pairs of data that are separated by τ). To increase the number of pairs and improve the statistics which contribute to the DCF, one often bins several lags together, i.e. all pairs of points in the interval $\tau - \delta$ to $\tau + \delta$ are binned together as one point. This increase the accuracy of the correlation amplitude but the resolution in time become worse.

time shift is referred to as the "lag" for a particular emission-line relative to the continuum. The Cross-Correlation Function (CCF) is defined as

$$F_{CCF}(\tau) = \int_{-\infty}^{\infty} L(t)C(t-\tau)dt \ . \tag{1.7}$$

Similarly, the continuum AutoCorrelation Function (ACF) is defined as

$$F_{ACF}(\tau) = \int_{-\infty}^{\infty} C(t)C(t-\tau)dt \ . \tag{1.8}$$

By using eq. 1.5 for $L(t)$ in eq. 1.7,

$$F_{CCF}(\tau) = \int_{-\infty}^{\infty} C(t-\tau)\int_{-\infty}^{\infty} \Psi(\tau')C(t-\tau')d\tau' dt \ , \tag{1.9}$$

and reversing the order of integration, we get

$$F_{CCF}(\tau) = \int_{-\infty}^{\infty} \Psi(\tau')\int_{-\infty}^{\infty} C(t-\tau')C(t-\tau)dt d\tau' \ , \tag{1.10}$$

where the interior integral is now recognized as eq. 1.8 for $F_{ACF}(\tau - \tau')$. Thus

$$F_{CCF}(\tau) = \int_{-\infty}^{\infty} \Psi(\tau')F_{ACF}(\tau-\tau')d\tau' \tag{1.11}$$

(Penston 1991). It can be seen that the CCF is a convolution of the transfer function and the continuum autocorrelation function. The lag for an emission-line is defined to be the location of the peak, or centroid, of the CCF $F_{CCF}(\tau)$. However, the lag measured depends not only on the transfer function, but also on the characteristics of the continuum variability, as seen from eq. 1.11. This was also demonstrated by Netzer (1991) for the data set of NGC 5548.

Cross-correlation techniques, that were previously used in astronomy for accurate radial velocity measurements, were first introduced by Gaskell and Spark (1986) for the above purpose. When dealing with actual observed light-curves, they are sets of numbers needed to be cross-correlated. Eq. 1.7 expressed as a sum of two unnormalized data set is

$$F_{CCF}(\tau) = \frac{1}{N\sigma_C\sigma_L}\sum_t C(t)L(t+\tau) \ , \tag{1.12}$$

radius. Also, as noted above, the response of all those geometries to a complicated change in the continuum can be obtained by integrating over the many δ-functions assembling it. From those simple examples it can be seen that for each geometry and change in the continuum flux, there is a unique response in the emission-lines. Therefore, knowing the continuum and line variability, the geometry of the BLR can be found. This was first introduced by Blandford and Mckee (1982) as finding the "transfer function".

The transfer function describes the response of an emission-line to a δ-function continuum outburst. The actual continuum behavior of AGNs is complex, and as a result the emission-line response is the convolution of the continuum variation and the transfer function. In general, the relationship between the continuum light-curve $C(t)$ (which reflect the changes of the continuum flux in time) and an emission-line light-curve $L(t)$ (which reflect the changes of the emission-line flux in time) can be described by

$$L(t) \ = \ \int_{-\infty}^{\infty} \Psi(\tau) C(t-\tau) d\tau \ , \tag{1.5}$$

which is known as the "transfer equation". The fundamental aim is to use the observables $C(t)$ and $L(t)$ to solve this integral equation for $\Psi(\tau)$, the transfer function, and thus infer the geometry of the BLR. In the original formulation of Blandford and Mckee (1982), the transfer function is obtained by Fourier methods using the convolution theorem

$$\tilde{\Psi}(\omega) \ = \ \frac{\tilde{L}(\omega)}{\tilde{C}(\omega)}, \tag{1.6}$$

where $\tilde{L}(\omega)$ is the Fourier transform of $L(t)$, etc., and then transforming $\tilde{\Psi}(\omega)$ back to the time domain. In real situations, solution by Fourier transforms does not work very well since the data are rarely even close to regularly sampled, and a very large number of points are required to obtain an accurate solution (in practice, a transfer function obtained this way has been published for only one data set of NGC 4151 by Maoz et al. 1991).

With data that are not well-sampled, it is possible to obtain some measure of the spatial extent of the BLR by cross-correlating the continuum and the emission-line light-curve in order to find the time shift between them that maximizes the correlation. This

the emitted-line fluxes. In the example of a thin shell geometry BLR, the response to a flash in the ionizing flux will be as follows: At time t after the flash a distant observer will see emission from a ring of radius $r\sin\theta$ centered on the line of sight, of area $2\pi r^2 \sin\theta d\theta$. Since we assume that the gas is optically thick to the ionizing continuum radiation, the energy dE emitted in the lines from the ring is proportional to its area, and the observed intensity I is

$$I(t) \;=\; \frac{dE}{dt} \;\propto\; \frac{\sin\theta d\theta}{dt} \;=\; const \;, \tag{1.2}$$

where the last equality is a result of eq. 1.1. Therefore the response of a shell to a short continuum burst is a "boxcar" function which is constant between $t = 0$, when the part of the BLR on the line of sight is responding, and $t = 2r/c$ when the far side of the BLR responds. This now can explain the result in the previous paragraph where a "boxcar" change in the continuum flux was assumed. By dividing this function into many δ-functions, each one producing a "boxcar" variation in the line flux, and summing all those "boxcars", we get the line variation response that was described in the previous paragraph.

The same calculation can be done for a ring-shaped BLR of radius r, with axis inclined at angle i to the line of sight. In cylindrical coordinates coaxial with the ring and origin at the ring center the delay of line emission emanating from a cloud at azimuthal angle ϕ on the ring is

$$t = \frac{r}{c}(1 - \sin i \cos\phi) \; . \tag{1.3}$$

The area of the ring seen by a distant observer during an interval dt is proportional to $d\phi$, hence

$$I(t) \;=\; \frac{dE}{dt} \;\propto\; \frac{d\phi}{dt} \;\propto\; \frac{1}{\sin\phi} \;=\; \frac{1}{\sqrt{1-\cos^2\phi}} \;=\; \frac{const.}{\sqrt{\sin^2 i - (1-\frac{ct}{r})^2}}$$
$$\text{for } \tfrac{r}{c}(1-\sin i) \leq\; t \leq \tfrac{r}{c}(1+\sin i), \text{ and 0 otherwise.} \tag{1.4}$$

In other words, the response has a double-peaked form centered at $t = r/c$.

The response of more complicated geometries, such as thick spherical shells and thin disks, to a short continuum flash can be calculate by integrating the above responses over

open questions in the AGN phenomenon. Studies of the extended structure (the NLR and beyond) show that on kiloparsecs scale AGNs are not spherically symmetric. The origin of this asymmetry is not known yet, is the continuum emission from the central source is anisotropy, or does the asymmetry caused by the BLR — by absorption or scattering of radiation in certain directions.

The small size of the BLR makes it impossible to get a direct picture, since even in the nearest AGNs the BLR is only several microarcseconds in size. However, it is possible to learn about the BLR in an indirect fashion, by studying the broad emission-line variability. This method is called "reverberation mapping" or "echo mapping", and entails detailed comparison of the continuum and the emission-line variation to determine the geometry and velocity field of the BLR (Peterson 1993). The first analysis of such reverberation in the emission-lines of AGNs was carried out by Bahcall, Kozlovsky, and Salpeter (1972), who calculated the response to the total line intensity in a spherical distribution of gas. They showed that because of the finite speed of light, an external observer will not see the the entire emission-line region responding instantaneously. A cloud at distance r from the central source and at angle θ to the line of sight will appear to respond after a time

$$t = \frac{r}{c}(1 - \cos\theta) \ . \tag{1.1}$$

The entire region will respond on a time scale characteristic of the light-travel-time across the region, r/c. For the spherical distribution of gas, when the recombination time is short, the response to ionizing flux which is constant except in a time interval $0 \leq t \leq \tau_{on}$, when it is larger by a constant factor A (a "boxcar"), the line intensity rises linearly with time for $0 \leq t \leq \tau_{on}$, is constant for $\tau_{on} < t < 2r/c$, and then decay to its original value in a time τ_{on}, where $r \geq c\tau_{on}/2$ is the radius of the shell.

The above is an example of a response of spherical BLR to a "boxcar" change in the ionizing flux. In order to calculate the response to a more complicated changes in the ionizing flux we need to check the response of the BLR to a flash in the ionizing flux, i.e. a δ-function, and then to look at the complicated change of the continuum as a sum of many δ-functions to gather the overall variability that will be observed from the BLR in

interaction of the radiation from the center with the atoms in the BLR and the NLR. Photoionization can explain most of the emission-line fluxes, and the line ratios. The continuum luminosity changes are explained as changes in the accretion rate of matter onto the black hole. The variable photoionizing flux results in flux variation of the broad emission-line, with a time delay characteristic to the size of the BLR (the light travel time from the central source to the BLR). Those changes are not seen in the narrow emission-lines since the NLR is three orders of magnitude larger than the BLR, hence the light travel time is too long. The NLR is relatively very large, so changes in the flux are smeared out and cannot be detected.

The photoionization model and the relative strength of the, broad lines, indicates that the gas temperature in the BLR is of order 1–3 $\times 10^4$ K and the particle density is $n \geq 10^9$ cm^{-3} (the typical gas density of the NLR is 10^3-10^6 cm^{-3} and the gas temperature is the same order as in the BLR). The large widths of the broad lines cannot be explained by thermal motion since the sound speed in a 10^4 K gas amount to only $\sim$ 10 km s^{-1}. A reasonable explanation for the large widths of the emission-lines is Doppler broadening due to bulk motion of the gas clouds. By assuming that the system of clouds emitting the lines is virialized, and by estimating the size of the BLR, one can find easily the central mass of the AGN — the mass of the black hole.

1.2 The BLR and its Mapping

The above argument demonstrate how important it is to understand the physics of the BLR. Since the central source is so compact and surrounded by gas clouds, it cannot be observationally resolved and studied directly. Thus, the BLR becomes the main probe of the inner regions of AGNs. The dynamics of the BLR is determined by forces related to the central source which are gravitation and pressure. Also, the emitted line spectrum offers a look into the ionizing continuum which is not observable in other ways. The physical structure of the BLR may provide information about the origin of its gas and about how the central source is fueled. Learning the BLR can also help in answering

clouds that are less densed and slower, which explain the narrowness of the forbidden-lines. The geometry of the NLR was resolved only in AGNs which are close to us (e.g. Evans et. al. 1993 found biconial structure for NGC 4151), but the geometry of the NLR in more distant AGNs is not known. Geometries that were offered for those regions are spheres, disks and toruses, all in different sizes.

There are attempts to unify several AGN subclasses into one model called *The Unified Scheme*. The basics of those models are the ones sketches in the previous paragraph. For example the attempt to explain Seyfert 1s and Seyfert 2s in one theory diverge into two directions. First approach suggests an obscuring torus surrounding the black hole and the BLR. When observing the AGN from the pole of the torus both the BLR and the NLR are seen and the AGN is classified as a Seyfert 1. When the AGN is observed from the plane of the torus, only the NLR is seen and the AGN is classified as a Seyfert 2. The second approach suggests time evolution of the nucleus activity for the unified model. When the nucleus activity is high both the BLR and the NLR are excited and emission-lines from both regions are seen. When the nuclear activity is at minimum the broad-lines disappear after a short time since the recombination time of the BLR is short due to its high density, but the low density gas in the NLR will show emission lines years afterwords since the recombination time is much longer. Hence, the object will turn from Seyfert 1 into Seyfert 2. More speculative attempts are to unify *all* AGN family members in one model called *Grand Unified theory* which uses several parameters to describe AGNs (mass, luminosity etc). However, the unification theories are yet very far from being complete since there are many features that cannot be explained by them (Blandford 1990, Netzer 1990).

As noted, according to the model the great amount of energy produced in AGNs is due to the accretion of matter onto the black hole which produce the continuum emission (There are alternative radiation processes that can produce the observed continuum but they all assumed to radiate the energy they are getting from the central source). The model explains the emission-lines observed as due to photoionization, caused by the

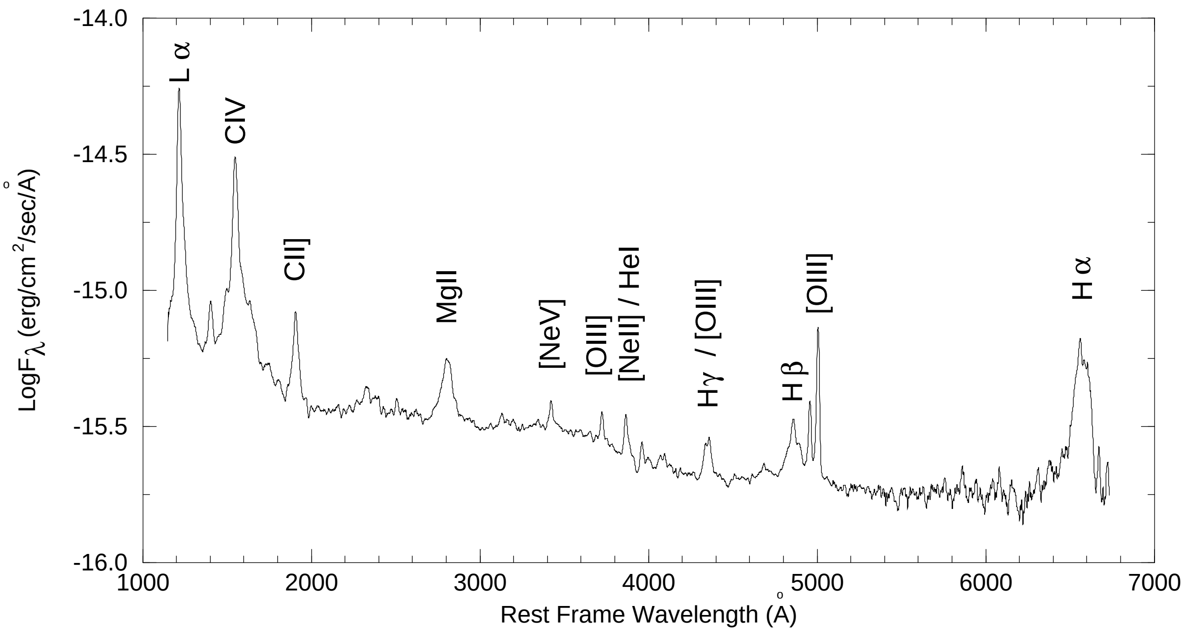

Figure 1.1: Spectrum of the radio-loud quasar 3C 215.

The above main features of AGNs are the fundamentals of a model that was developed to explain the AGNs phenomenon. This model includes a black hole in the center of the AGN, which is fed by an accretion disk. The energy produced in the process of accreting matter into the black hole can explain the huge amount of energy observed from the AGN as continuum emission. At a distance of $\sim$ 0.1 pc from the central source there is the "Broad Line Region" (BLR) which is the region emitting the broad emission-lines. Further away from there, at a distance of $\sim$ 100 pc, We find the "Narrow Line Region" (NLR) which is responsible to the emission of the narrow emission-lines. The BLR (and the NLR in quasars) cannot be resolved in astronomical observations, and the main and only information about them comes from the emission-lines. The elements composing the material in the BLR and the NLR are known from the emission-lines, but the geometry of those regions (excluding Seyferts NLRs) cannot be seen and hence is not known. Some models suggest giant stars for the BLR clouds, others assume small or big densed gas clouds, all moving very fast around the black hole. For the NLR, the model suggests gas

There are two prominent components in AGN spectra. The first is the nonstellar continuum spectrum which can be fitted, on different and limited wavelength ranges, with a simple power law: $F_\nu \propto \nu^{-\alpha}$, where F_ν is the monochromatic flux at frequency ν. α, the spectral index, is different for each wavelength range and subclass, but in many AGNs (in particular quasars and Seyfert 1) it was found that $\alpha \approx 1 - 1.2$ in the IR range, $\alpha \approx 0.3 - 0.7$ in the optical, and $\alpha \approx 0.7$ at the hard X-ray range. In the radio wavelength range, the continuum emission is divided into two categories "steep spectrum" and "flat spectrum", with the separation taken around $\alpha \approx 0.4$ (at 1 GHz).

The second component in the spectrum consist of the emission lines. The common emission-lines are of hydrogen ($L\alpha$, $H\alpha$ and $H\beta$), oxygen (e.g. $OVI\lambda1035$, $[OIII]\lambda5007$), carbon (e.g. $CIII\lambda977$, $CIV\lambda1549$, $CIII]\lambda1909$), helium, magnesium and many iron lines. The width of the emission-lines is divided into two categories: broad emission-lines with $3000 < FWHM < 10,000$ km s^{-1}, and narrow emission-lines with $300 < FWHM < 1000$ km s^{-1}. Quasar spectra have broad permitted emission-lines and narrow forbidden emission-lines while in LINERs spectra all emission-lines are narrow. The division into broad and narrow emission lines is the basic method to distinguish Seyfert 1s from Seyfert 2s galaxies. Seyfert 1s have broad permitted emission-lines and narrow forbidden emission-lines, hence their spectrum resemble the quasars spectrum (but with two order of magnitude lower in luminosity). Seyfert 2s show only narrow emission-lines, hence their spectrum resemble the LINERs spectrum (but with two orders of magnitude higher in luminosity). A typical spectrum of radio-load quasar (3C 215) is illustrated in Figure 1.1, where the distinction between broad-lines (e.g. $H\alpha$, $H\beta$) and narrow-lines (e.g. $[OIII]$) is very clear.

From repeated observations of AGNs in the past decade, it was found that the luminosity of some of those objects is changing on different time scales. Furthermore, it was found that changes in the intensity of the continuum flux often followed by corresponding changes in the strength of the broad emission-lines. This will be further discused in the following sections.

Chapter 1

Introduction

1.1 Active Galactic Nuclei

Active Galactic Nuclei (AGNs) are a class of astronomical objects that have been under extensive study in the past three decades. The uniqness of the objects in this class is that they have very high energy output (i.e. more than the output energy of galaxies). Also, they show energetic phenomena whose origin is not due to stellar processes, i.e. not from nucleusynthesis, blackbody radiation, etc. Examples for such phenomena are: high energy output from a very compact nuclear region in a galaxy, nonstellar continuum emission and nuclear emission-lines excited by this continuum.

The class of AGNs includes many subclasses that were defined in different ways and in different astronomy wavelength bands — radio astronomy, optical astronomy etc. At the high luminosity end we find the quasars (radio loud and radio quiet) with luminosity of order 10^{46} erg s^{-1} (and redshifts between $1-5$). At the middle energy scale there are the Seyfert galaxies which are divided into two types: type 1 with luminosity of $\sim 10^{44}$ erg s^{-1}, and type 2 with $\sim 10^{43}$ erg s^{-1} (most of the Seyfert galaxies have redshift less than 1). At the very faint end there are the Low Ionization Nuclear Emission Line Regions (LINERs) with luminosity of order 10^{41} erg s^{-1} (LINERs are all very close objects). There are more subclasses like BL-Lac objects, Optically Violent Variables (OVVs), Star-burst galaxies and others (Lawrence 1987, Woltjer 1990), but the ones mentioned above are the most numerous.

Abstract

This work reports on the two year spectrophotometrical monitoring program of a subsample of 28 of the Palomar-Green Bright Quasar Sample. The program's aims were to test for correlations between continuum and emission-line variations and to determine the timescales relevant to mapping the Broad Line Regions (BLRs) of high-luminosity Active Galactic Nuclei (AGNs).

Half of the quasars showed optical continuum variations with amplitudes in the range of 20-75%. The rise and fall time for the continuum variations is typically 0.5-2 years. In most of the objects with continuum variations, correlated variations was detected in the broad $H\alpha$ and $H\beta$ emission lines. The amplitude of the line variations is usually 2-4 times smaller than the optical continuum fluctuations.

Light curves and analyzed spectra are presented for six of the variable quasars with 1000-10000Å luminosity in the range of 0.3–4$\times10^{45}$ erg s^{-1}. In four of these objects the lines respond to the continuum variations with a lag that is smaller than or comparable to the typical sampling interval (a few months). The observational results were analyzed using the cross-correlation method and Monte-Carlo simulations. It was established that the variation in the emission-lines lag behind the continuum variations with a time lag of order 70 days, indicating a BLR with a typical size of 70 light-days. In addition, preliminary results show that the BLR size of AGNs scales with luminosity.

Two of the quasars monitored show no detectable line variations despite relatively large-amplitude continuum changes. This could be a stronger manifestation of the low-amplitude line-response phenomenon observed in the other quasars.

A new method that was not attempted before, of "geometric series simulation" is presented in this study. It enables examination of the BLR geometry by changing one parameter in the geometry. It was found that for a model with a covering factor given by $dc \propto r^{-5/6}$, the observations of the PG quasars are consistent with a thick shell BLR with thickness of few hundred light-days.

Contents

Acknowledgements

I wish to thank my supervisor, Professor Hagai Netzer for his guidance, support and encouragement in the course of this work.

I also thank Doctor Dan Maoz for his support and many enlightening discussions, and for introducing me to the observational work.

I have benefited from help and discussions with my fellow students Tal Alexander, Benny Belinko, and Oleg Goldshmidt.

I am indebted to the Wise Observatory staff: Ezra Mashal, Sammy Ben-Guigui, Peter Ibbetson and John Dan, for their assistance with the observations, and to Ana Heller and Friedel Loinger for their help with computer matters.

My wife Shula deserves special thanks for her unlimited patience and support during the past two years.

TEL-AVIV UNIVERSITY

RAYMOND & BEVERLY SACKLER

FACULTY OF EXACT SCIENCES

EMISSION LINE VARIABILITY IN PALOMAR-GREEN QUASARS

THESIS SUBMITTED FOR THE M.Sc. DEGREE

AT TEL-AVIV UNIVERSITY

SCHOOL OF PHYSICS AND ASTRONOMY

by

Shai Kaspi

This work was carried out under the supervision of

Professor Hagai Netzer

March 1994